

1 **Interannual Variation and Trend of Carbon Budget Observed Over a 28-**  
2 **year Period at Takayama in a Cool-Temperate Deciduous Forest in Central**  
3 **Japan**

4  
5 **Shohei Murayama<sup>\*1</sup>, Hiroaki Kondo<sup>1,2</sup>, Shigeyuki Ishido<sup>1</sup>, Takahisa Maeda<sup>1</sup>, Nobuko**  
6 **Saigusa<sup>3</sup>, Susumu Yamamoto<sup>1</sup>, Kazuki Kamezaki<sup>1</sup>, and Hiroyuki Muraoka<sup>4,5,6,3</sup>**

7  
8 <sup>1</sup> National Institute of Advanced Industrial Science and Technology (AIST), Tsukuba, Japan

9 <sup>2</sup> Japan Weather Association, Tokyo, Japan

10 <sup>3</sup> National Institute for Environmental Studies, Tsukuba, Japan

11 <sup>4</sup> River Basin Research Center, Gifu University, Gifu, Japan

12 <sup>5</sup> Center for Carbon Neutrality, Environment and Energy, Gifu University, Gifu, Japan

13 <sup>6</sup> Regional Adaptation Research Center, Gifu University, Gifu, Japan

14  
15 \*Corresponding author: Shohei Murayama ([s.murayama@aist.go.jp](mailto:s.murayama@aist.go.jp))

16  
17 **Key Points**

- 18 • Interannual variations and significant trends of carbon budget components at a forest site were  
19 detected from a long-term observation.  
20 • Environmental factors governing the interannual variations and the trend of the annual carbon  
21 budget components were investigated.  
22 • Some of the decadal scale phenomena obtained from this study could not be found without the  
23 long-term observation.

## 24 **Abstract**

25 Long-term carbon dioxide (CO<sub>2</sub>) flux measurements between the atmosphere and the  
26 ecosystem have been made since 1993 at a cool-temperate deciduous forest site (Takayama) in  
27 Japan influenced by Asian Monsoon, constituting the longest dataset among all the AsiaFlux  
28 sites. Interannual variations (IAVs) and trends of the annual carbon budget components and  
29 their environmental factors were examined. Annual net ecosystem production (NEP) (mean ±  
30 1σ) during the period of eddy covariance measurement in 1999-2021 was 265 ± 86 gC m<sup>-2</sup> yr<sup>-1</sup>,  
31 and its IAV was dependent more on gross primary production (GPP) than on ecosystem  
32 respiration. IAVs in annual NEP and GPP were correlated with the IAVs of the monthly mean  
33 NEP, GPP and leaf area index (LAI) from June to September, as well as with that of the length  
34 of the net carbon uptake period. Significant increasing and decreasing trends in the annual NEP  
35 and GPP were detected during 2004-2013 and 2013-2021, respectively; the increasing trends  
36 were mainly caused by the vegetation recovery from typhoon disturbances while the decreasing  
37 trends were partly influenced by recent extreme weather events. Significant positive  
38 correlations of the IAVs between the start and the end of the net carbon uptake period, and  
39 between the leaf expansion and leaf fall were found. These may be attributed to biological  
40 functions and interseasonal relationship of meteorological parameters associated with ENSO  
41 events that can also influence IAVs in annual NEP and GPP.

42

## 43 **Plain Language Summary**

44 Forest ecosystems play an important role in the global carbon cycle. However, time  
45 variations in the ecosystem carbon budget and its responses to climate change are not well  
46 understood. Although long-term observational data are useful for a better understanding, >20-  
47 year observations are limited, especially in the Asian monsoon region. In this study, long-term  
48 measurements of carbon budget made at a cool-temperate deciduous forest in Japan were  
49 analyzed for interannual variation (IAV), long-term trends, and offered plausible causes for  
50 these changes. The IAV in annual net carbon uptake (NEP) was associated with the variation in  
51 summertime NEP, as well as with the variation in the length of the net carbon uptake period  
52 (NGP). The IAV in summertime NEP was associated with the variations in solar radiation (SR)  
53 and leaf density during the season, while the IAV in NGP length depended on the variations in  
54 spring temperature and early-fall SR. Decadal increasing and decreasing trends of annual NEP  
55 were also detected. The former was mainly caused by recovery from typhoons, while the latter  
56 was likely related to recent extreme weather events. Longer-term ecosystem observations are  
57 certainly needed for more accurate predictions of forest ecosystems response to climate change.

58

## 59 **1. Introduction**

60 Terrestrial biosphere is one of the most important reservoirs in the global carbon cycle.  
61 Various changes in terrestrial biosphere caused by climate change and atmospheric carbon

62 dioxide (CO<sub>2</sub>) increase have been discussed in many recent studies (e.g., Friedlingstein et al.  
63 2022; Piao et al. 2019a; Reichstein et al. 2013). Extension of the growing season due to warmer  
64 climate and enhanced fertilization effects have caused increase in CO<sub>2</sub> uptake by the terrestrial  
65 ecosystems, while enhancement of respiration and decomposition of organic matters due to  
66 warmer climate have resulted in an increase in CO<sub>2</sub> release (IPCC, 2021). On a shorter and local  
67 scale, disturbance of ecosystem functions due to increase in frequency of extreme weather  
68 accompanied by climate change can affect the carbon budget (e.g., Reichstein et al. 2013).  
69 Given that East Asia is strongly influenced by the Asian Monsoon, any change in the  
70 temperature and precipitation amount, along with the length of the rainy season, associated with  
71 the monsoon can have a major impact on the terrestrial carbon budget. The present research  
72 addresses some of these issues.

73 Various networks of CO<sub>2</sub> flux measurements between the atmosphere and the terrestrial  
74 ecosystems have been developed since 1990's (e.g., Wofsy et al., 1993; Baldocchi et al., 2001).  
75 Understanding of the environmental factors causing carbon flux changes and the development  
76 of terrestrial carbon cycle models all benefited from the measurements obtained from these  
77 networks (e.g., Musavi et al., 2017). In particular, long-term data are employed to contribute to  
78 the reduction of uncertainty in statistical analyses of the interannual variations (IAV) and the  
79 secular trend (Baldocchi et al., 2018). Thus, decadal-scale study should be conducted by  
80 combining micro-meteorological observation and ecological research (Ito et al. 2015; Muraoka  
81 et al. 2015). However, the long-term measurements of >20 years are still limited, especially in  
82 the Asian monsoon region.

83 Long-term measurements of CO<sub>2</sub> flux between the atmosphere and the forest ecosystem,  
84 and the atmospheric CO<sub>2</sub> mixing ratio in and above the canopy have been made since September  
85 1993 at Takayama site (TKY) in a cool-temperate deciduous forest in central Japan (Yamamoto  
86 et al., 1999; Saigusa et al., 2002; Murayama et al., 2003). TKY has the longest flux data among  
87 the AsiaFlux sites (<https://www.asiaflux.net/>). Also, the continuous measurement of the  
88 atmospheric O<sub>2</sub>/N<sub>2</sub> ratio, along with the measurement of the atmospheric CO<sub>2</sub> isotopic ratios  
89 using a flask sampling method have been conducted at the site (Ishidoya et al., 2015; Murayama  
90 et al., 2010). Various analyses of the data have been conducted to obtain a better understanding  
91 of the IAV in annual carbon budget related to Asian Monsoon and ENSO events (Saigusa et al.,  
92 2005, 2008; Yamamoto et al., 1999).

93 In this study, the longer-term data between 1994 and 2021 (mainly between 1999 and 2021)  
94 are reanalyzed to investigate the decadal changes in the IAV and the trend of annual carbon  
95 budget associated with observed climatic and ecological mechanisms. We will examine the  
96 relationship of the IAV in the annual carbon budget with those in the summertime carbon uptake  
97 (Subsection 4.1) and the net carbon uptake period (Subsection 4.2), on the assumption that the  
98 annual carbon budget is largely affected by these parameters. We will further examine the trend  
99 of the annual carbon budget and its causes, such as disturbances of the forest and meteorological

100 trends (Subsection 4.3). We will also examine the impact of recent extreme weather on the  
101 carbon budget. Based on these results, climatic and ecological mechanisms governing the IAV  
102 (Subsection 5.1) and the trend (Subsection 5.2) of the annual carbon budget will be discussed  
103 by comparing with the previous studies of other forest sites, as well as TKY. We will also discuss  
104 influences of interseasonal factors and El Niño-Southern Oscillation (ENSO) on the IAV and a  
105 decadal trend of the annual carbon budget (Subsection 5.3).

106

## 107 **2. Method**

### 108 **2.1. Site descriptions**

109 Detailed descriptions of our observation site have already been given in our previous papers  
110 (Yamamoto et al., 1999; Saigusa et al., 2005; Murayama et al., 2010). Our observation site,  
111 TKY is located in a mountainous area in the central part of the main island of Japan (36°09'N,  
112 137°25'E, 1420 m a.s.l.) and is situated about 15 km east of a local city, Takayama. TKY is part  
113 of observation networks such as AsiaFlux ([http://asiaflux.net/index.php?page\\_id=112](http://asiaflux.net/index.php?page_id=112)) and  
114 Japan Long-Term Ecological Research network (JaLTER: <http://www.jalter.org/en/>).  
115 Vegetation at the site is a 60 to 70-year-old secondary deciduous broadleaf forest primarily  
116 dominated by birch (*Betula ermanii* Cham and *B. platyphylla* Sukatchev var. *japonica* Hara)  
117 and oak (*Quercus crispula* Blume). The canopy height is about 15-20 m. The forest understory  
118 is dominated by an evergreen dwarf bamboo (*Sasa senanensis* Rehd.) (Muraoka & Koizumi,  
119 2005; Ohtsuka et al., 2007). Leaf expansion and leaf fall of broadleaf trees occur in May and in  
120 October or November, respectively, and the ground surface is usually covered with snow from  
121 December to April. Annual mean temperature and precipitation amount averaged over 1994-  
122 2021 are about 6.7°C and 2200 mm, respectively. The rainy season is strongly influenced by  
123 the Asian Monsoon and usually occurs in early summer (June – July). Possible effects of nearby  
124 anthropogenic sources on the data observed at our site were estimated by Kondo et al. (2001)  
125 using a numerical model and were found to be relatively minimal.

### 126 **2.2. Observation**

127 Since detailed descriptions of our CO<sub>2</sub> flux and atmospheric CO<sub>2</sub> mixing ratio  
128 measurements have been given in our previous papers (Yamamoto et al., 1999; Saigusa et al.,  
129 2002, 2005; Murayama et al., 2003, 2010), only a brief and supplemental explanation will be  
130 presented here.

131 The continuous measurements of the CO<sub>2</sub> flux and the atmospheric CO<sub>2</sub> mixing ratio have  
132 been made using a 27-m height tower located on the top of a small hill. Meteorological  
133 parameters such as downward and upward shortwave and longwave radiations, air temperature,  
134 relative humidity, wind speed, and its direction were also measured on the tower. Photosynthetic  
135 active radiation (PAR) was measured above and below the tree canopy (but above the canopy  
136 of dwarf bamboo) using quantum sensors (IKS-27, KOITO and/or SQ-110, APOGEE). The  
137 daily LAI of the tree canopy not including the dwarf bamboo was estimated as follows:

138

$$LAI = -\frac{1}{K} \left( \ln \frac{PAR_b}{PAR_a} - \ln \frac{PAR_{b0}}{PAR_{a0}} \right), \quad (1)$$

139

140

141

142

143

144

145

146

147

148

where  $PAR_b$  and  $PAR_a$  denote daily summed values of the downward PAR measured below and above the canopy,  $PAR_{b0}$  and  $PAR_{a0}$  denote those averaged for the period of DOY (day of the year) 100-120 before starting leaf expansion, and  $K$  denotes the extinction coefficient. Here, we set  $K$  to a constant value (0.46) based on the estimation for TKY (Muraoka et al., 2010; see also Nasahara et al. 2008, Saitoh et al. 2012). The obtained LAI values were often scattered day by day. Therefore, we used their 10-day running mean values for the further analyses in relation to the  $CO_2$  flux. Since some problems with the PAR measurement below the tree canopy occurred in 2019, the LAI data for the year were not used for analyses in this paper. Precipitation was measured at a site located about 400 m from the tower by the River Basin Research Center (RBRC), Gifu University.

149

150

151

152

153

154

155

156

157

158

The  $CO_2$  flux measurement started by an aerodynamic (AD) method and an eddy covariance (EC) method in September 1993 and July 1998, respectively. The hourly  $CO_2$  flux by AD method was estimated from the vertical gradient of the hourly mean  $CO_2$  mixing ratio between two heights above the canopy (27 and 18 m). The  $CO_2$  mixing ratio was measured by a non-dispersive infrared (NDIR) analyzer (Model 880, Rosemount or LI-6252, Li-Cor) with precision of better than 0.1 ppm. The  $CO_2$  flux data by the AD method were intensively compared with those by the EC method between July 1998 and December 2000 (Saigusa et al., 2005). The relationship between both methods was obtained from the comparison of the daily values. The daily  $CO_2$  flux data by the AD method were adjusted to those by the EC method using the relationship during the period before the start of the EC measurement.

159

160

161

162

163

164

165

The  $CO_2$  flux measurement by the EC method at 25 m on the tower was made using a three-dimensional ultrasonic anemometer (DAT-600, Kaijo) and a closed-path NDIR (LI-6262, Li-Cor). Detailed descriptions of the eddy covariance method were given in Saigusa et al. (2002). The net ecosystem  $CO_2$  exchange (NEE) was calculated every half-hour taking account of the  $CO_2$  storage in the canopy. Small data gaps of up to 2-3 h were filled by linear interpolation. Large gaps were filled by empirical equations expressing the relationship among NEE, air temperature and incident PAR above the tree canopy shown in Saigusa et al. (2002, 2005).

166

167

168

169

170

171

172

173

174

Drainage flow along the slope often occurred in calm nights at TKY, and the NEE measured by the EC method was likely underestimated during the nighttime under the stable atmospheric conditions. To avoid the flux underestimation, the NEE values at the stable nights had been replaced by an empirical exponential formula throughout the year obtained from the relationship between the air temperature at 25-m height and the ecosystem respiration ( $Rec$ ) at the site measured by the eddy covariance method under nearly neutral atmospheric stability conditions in Saigusa et al. (2002, 2005). In this study, the relationship between the air temperature ( $T$  (°C)) at 25-m height and  $Rec$  ( $\mu mol\ m^{-2}\ s^{-1}$ ) was reanalyzed using the long-term data. Because its seasonal difference of the relationship was found from the reanalysis, the

175 following empirical formulas were used to estimate *Rec* (nighttime NEE) under the stable  
176 atmospheric conditions (friction velocity ( $u^*$ )  $< 0.5 \text{ m s}^{-1}$ ) for each period of the year:

177  $Rec = 2.37 \times 3.42^{\frac{T-10}{10}} (T < 15), Rec = 4.39 (T \geq 15)$ , for April and May, (2)

178  $Rec = 0.0821T + 2.74$ , for June and July, (3)

179  $Rec = 0.110T + 1.59$ , for August and September, (4)

180  $Rec = 2.11 \times 1.87^{\frac{T-10}{10}} (T < 16), Rec = 3.06 (T \geq 16)$ , for October and November, (5)

181  $Rec = 0.0232T + 0.667$ , for December to March. (6)

182 In this study, we assumed that the temperature dependence of daytime *Rec* was the same as that  
183 of nighttime *Rec*, though problems with the assumption have been pointed out in some studies  
184 (e.g., Reichstein et al., 2005; Wehr et al., 2016).

185 In the following analyses, daily (24 h) carbon budget components were calculated as  
186 follows. The daily net ecosystem production (NEP) was assumed to be the negative quantity of  
187 the daily NEE:

188  $NEP = -NEE$ . (7)

189 The daily gross primary production (GPP) was derived from NEP and *Rec*:

190  $GPP = NEP + Rec$ . (8)

191

### 192 **3. Data analyses**

193 In order to examine the IAV in the seasonal cycle of NEP, we obtained the best fit curve to  
194 the daily NEP data by employing the curve fitting technique described in Nakazawa et al. (1997).  
195 In this iterative procedure, the fundamental and its first to third harmonics (a four-harmonic fit)  
196 were used.

197 The occurrences of the NEP growing start (NGS) and end (NGE) were defined by the  
198 intersections of the above-mentioned best fit curve and the zero line from the negative value to  
199 the positive one (net CO<sub>2</sub> release to uptake) and from the positive value to the negative one (net  
200 CO<sub>2</sub> uptake to release), respectively. The interval between the NGS and the NGE, which is the  
201 net carbon uptake period, was also defined as the NEP growing period (NGP).

202

### 203 **4. Results**

204 In Fig. 1a, the daily NEP and the best fit curve to these data are shown for 1994-2021.  
205 Although day-to-day NEP is largely scattered, the NEP often shows positive values (CO<sub>2</sub>  
206 uptake) and negative values (CO<sub>2</sub> release) from late spring to early fall and the remaining period,  
207 respectively. Obvious positive peaks in summer and large IAV in the peak height are seen from  
208 the fitting curve. On the other hand, relatively weak CO<sub>2</sub> release is seen from late fall to early  
209 spring, and the IAV in the CO<sub>2</sub> release during these periods is very smaller than that in the CO<sub>2</sub>  
210 uptake peak.

211 Figure 1b shows temporal variations of monthly mean of the estimated carbon budget  
 212 components. The monthly mean data are also given in the Supporting Information (Tables S1-  
 213 S3). Each component has sharp peaks in summer and broad troughs in cold seasons, though  
 214 small sharp troughs are seen late in fall and/or in early spring in some years. The IAV in the  
 215 summer peak height of GPP is larger than that of Rec. Therefore, the IAV in the summer peak  
 216 height of NEP is mainly due to that of GPP.

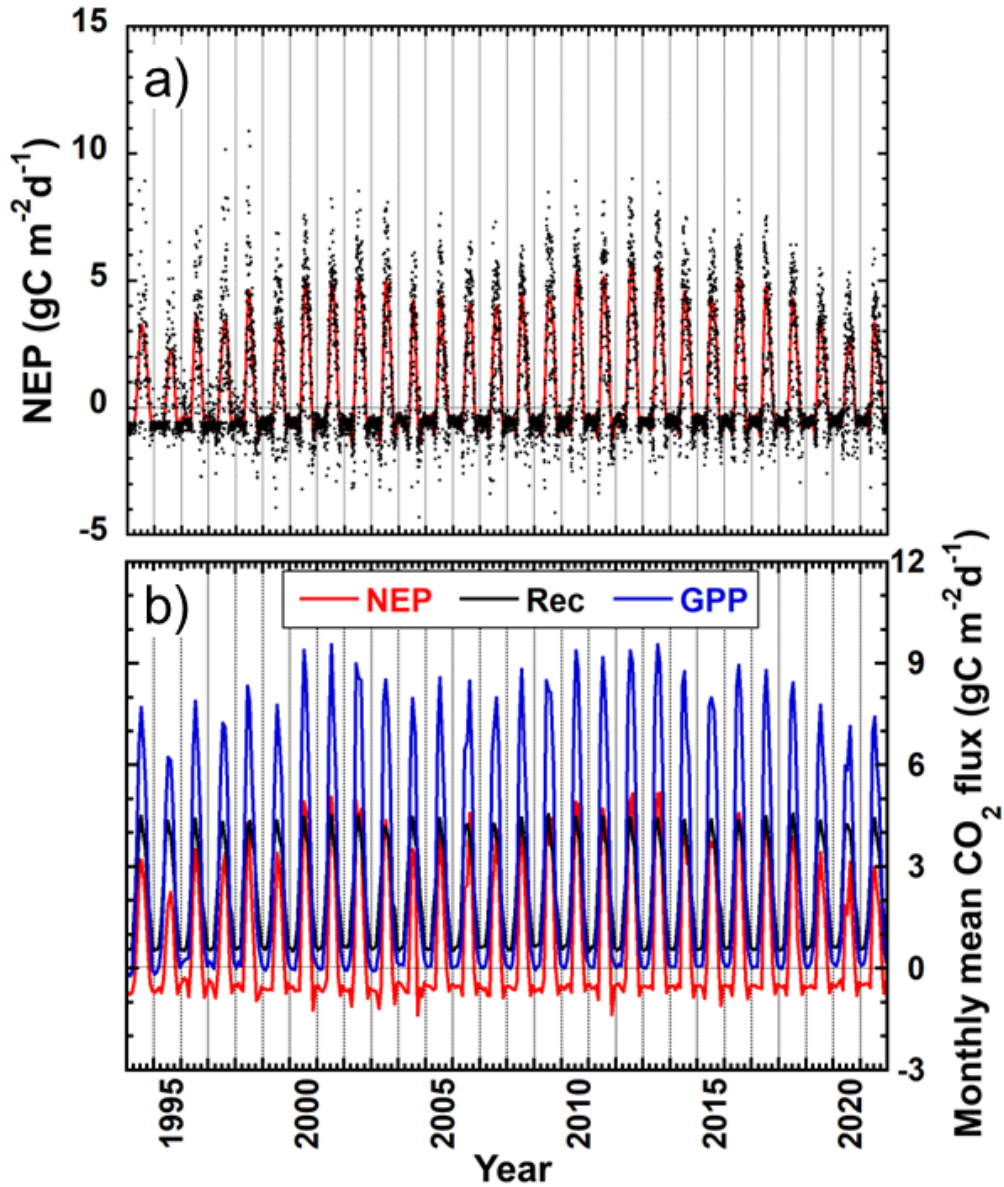


**Figure 1.** a) Temporal variation in daily NEP (dot) and the best fit curve to the data (red line) for 1994-2021. b) Temporal variations in monthly mean daily NEP (red line), Rec (black line) and GPP (blue line) for the same period.

217

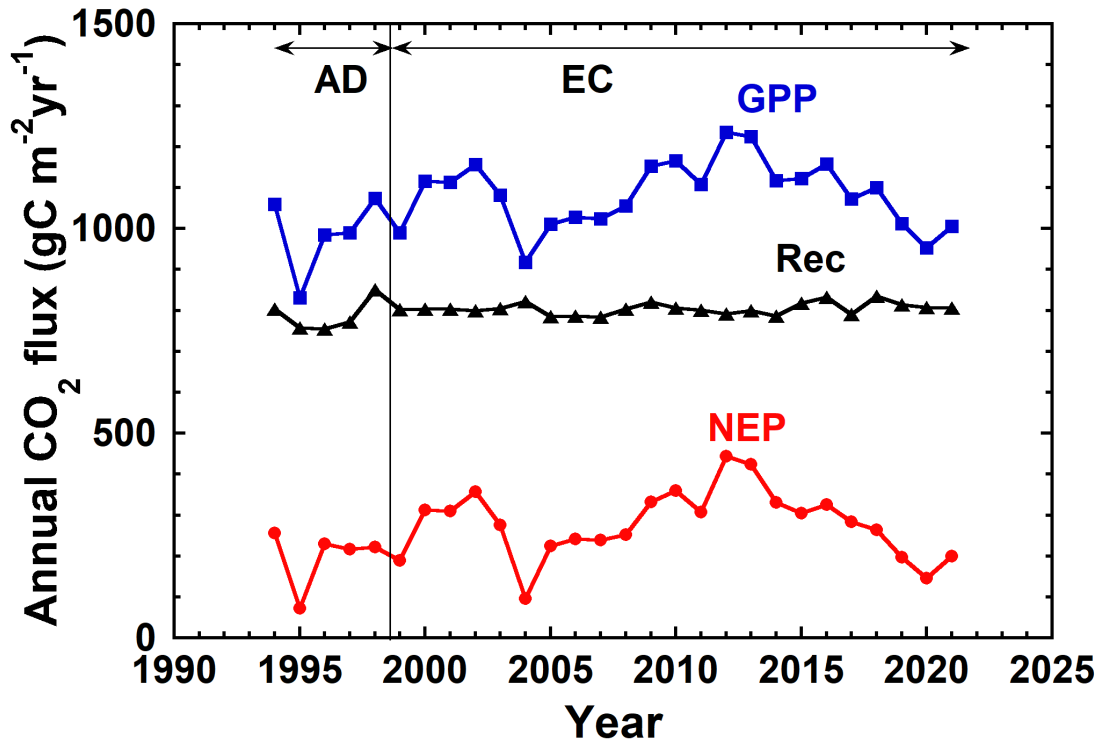


**Figure 2.** Temporal variations in annual NEP, Rec and GPP. The data were obtained by using an aerodynamic (AD) method and an eddy-covariance (EC) method until July 1998 and after that, respectively.

218 Figure 2 shows variations of the estimated annual carbon budget components. The data of  
 219 the annual carbon budget components are also given in the Supporting Information (Table S1-  
 220 S3). The IAV is much larger for annual NEP and GPP than for annual Rec. The average values  
 221 and the standard deviations ( $1\sigma$ ) of annual NEP, GPP and Rec for 1994-2021 were  $265 \pm 86$ ,  
 222  $1066 \pm 91$ , and  $801 \pm 21$   $\text{gC m}^{-2} \text{yr}^{-1}$ , respectively. For the EC observation period of 1999-2021,  
 223 they were  $279 \pm 83$ ,  $1083 \pm 82$ , and  $804 \pm 14$   $\text{gC m}^{-2} \text{yr}^{-1}$ , respectively. The fact that the IAV  
 224 pattern of the annual NEP is similar to that of the annual GPP suggests that the IAV in the annual  
 225 NEP depends largely on the IAV in the annual GPP at TKY. The annual NEP and GPP both  
 226 show increases from the late 1990s to early 2000s, rapid decreases in 2004, gradual increases  
 227 from 2004 to the early 2010s, and then gradual decreases in the late 2010s. The rapid decreases  
 228 of the annual NEP and GPP in 2004 were related to disturbances of the forest ecosystem due to  
 229 typhoon strikes, as suggested by fairly lower LAI values from June to October in 2004  
 230 compared to the averaged values (Fig. S1). Ten typhoons landed in the Japanese Islands from  
 231 June to October in that year (Ito, 2010a), which were more than three times the average annual  
 232 landfalls in Japan over the 1991-2020 period  
 233 ([https://ds.data.jma.go.jp/gmd/cpd/longfcst/en/tourist\\_tc.html](https://ds.data.jma.go.jp/gmd/cpd/longfcst/en/tourist_tc.html)).

234 The IAVs of the maximum NEP during the summertime and the length of the NGP can  
 235 strongly influence the IAV of the annual NEP, as illustrated in Fig. 3. In the following sections,  
 236 factors governing IAVs and trends of annual carbon budget components will be analyzed based  
 237 on this concept. To avoid systematic difference between AD and EC measurements, the  
 238 following statistical analyses of the carbon budgets will mainly employ the EC data obtained  
 239 during the period of 1999-2021. Some statistical analyses will be limited to 1999-2017 to

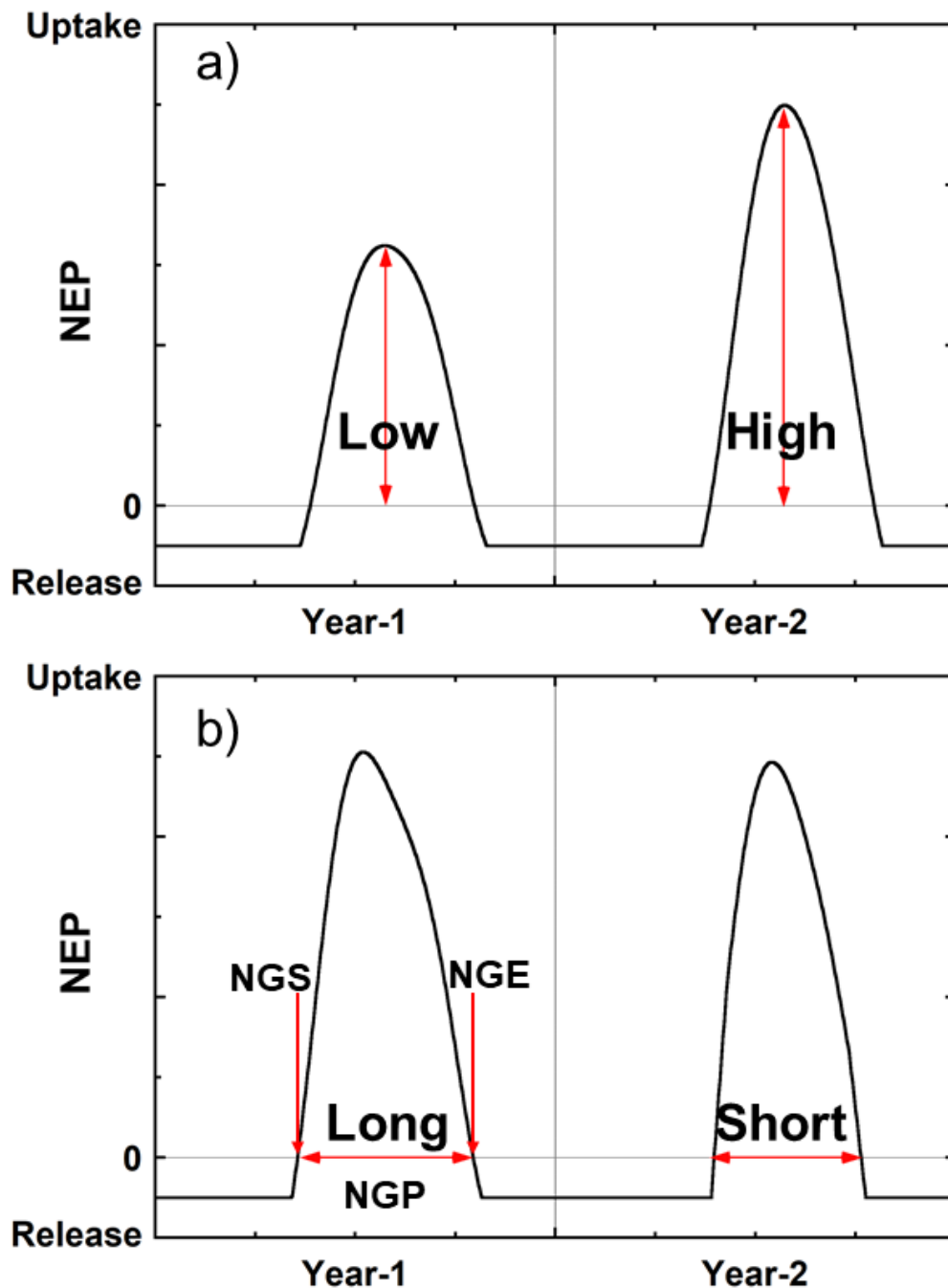


**Figure 3.** Schematic diagram showing factors governing the IAV in annual NEP; a) the IAV in the magnitude of the NEP during the summertime, and b) that in the length of the period (NGP) showing positive NEP values (between the NGS and the NGE).

240 exclude possible impacts of increase in the frequency of recent extreme weather events  
 241 described later.

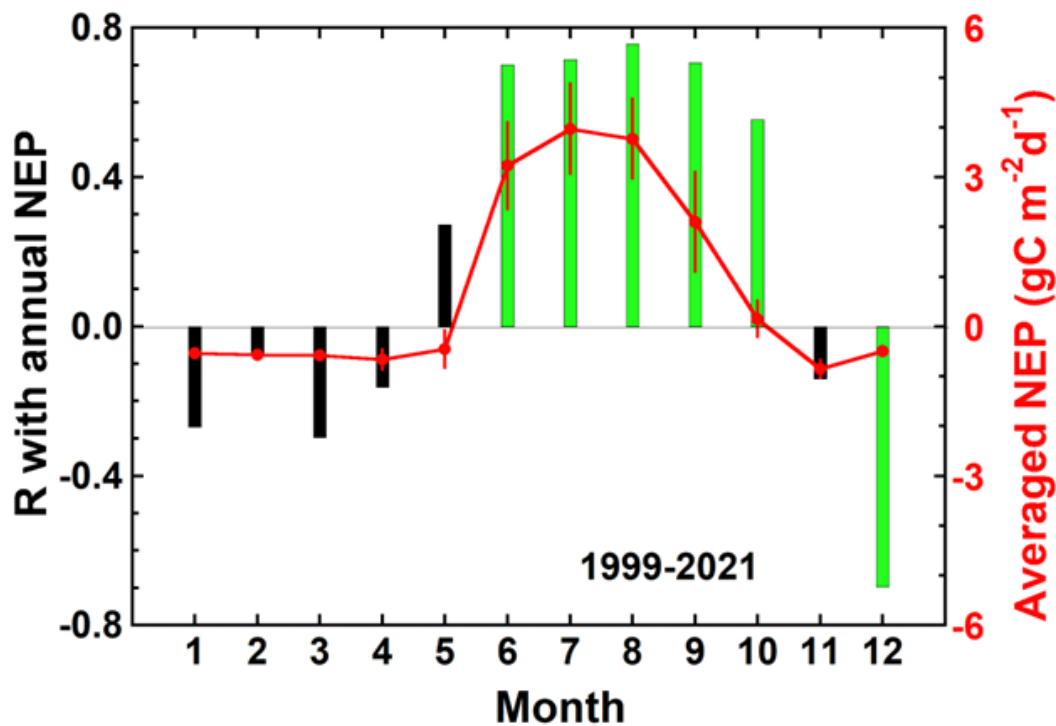


**Figure 4.** Correlation coefficients (R) of the IAV between annual NEP and monthly mean NEP for each month for 1999-2021 (green and black vertical bars), and the averages of monthly mean NEP for each month over 1999-2021 (red closed circles) along with the standard deviation ( $1\sigma$ ) from the average values (red vertical lines). The green bars represent significant correlations at >99% confident levels.

242

#### 243 **4.1. Influence of summertime IAV in carbon uptake on annual NEP and GPP variability**

244

245

246

247

248

249

250

251

252

253

254

255

Since photosynthetic activities are largely enhanced during the summertime, it can be hypothesized that the IAV in strength of carbon uptake in summer contributes to the IAVs of the annual NEP and GPP. To examine this hypothesis, correlations of the IAV between the annual NEP and monthly mean NEP for each month were analyzed for the period 1999-2021. In Fig. 4, the correlation coefficients (R) for each month are shown. The average values of monthly mean NEP, along with the standard deviation ( $1\sigma$ ) from the average values, are also shown in this figure. With the exception of December, statistically significant positive correlations of the IAV between the annual NEP and monthly mean NEP for each month from June to October are found ( $P < 0.01$ ). Especially from June to September, the average values of the monthly mean NEP show large net CO<sub>2</sub> uptake ( $> 2 \text{ gC m}^{-2} \text{ d}^{-1}$ ) and IAV ( $\sigma > 0.8 \text{ gC m}^{-2} \text{ d}^{-1}$ ). Similar significant correlations ( $P < 0.01$ ) of the IAV were found between annual GPP and monthly mean GPP for each month from June to September, when the average values of the

256 monthly mean GPP ( $>5 \text{ gC m}^{-2} \text{ d}^{-1}$ ) and the IAVs ( $\sigma > 0.8 \text{ gC m}^{-2} \text{ d}^{-1}$ ) were large. These results  
 257 suggest that the IAVs in NEP and GPP from June to September make significant contributions  
 258 to the IAVs observed in annual NEP and GPP.

**Table 1.** Correlation coefficient of IAVs of monthly mean SR in June, July, August and  
 September with those of monthly mean NEP and GPP for the respective months in 1999-  
 2021 and 1999-2017 except for 2004.

259

	June	July	August	September
NEP 1999-2021	0.22	0.67***	0.46**	0.64***
1999-2017	0.31	0.62***	0.68***	0.58**
GPP 1999-2021	0.22	0.71***	0.51**	0.59***
1999-2017	0.30	0.65***	0.70***	0.50**

Note: \*\* and \*\*\* represent statistical significance of correlations for  $0.05 < P \leq 0.01$  and  $P < 0.01$ , respectively.

260

261 Table 1 shows correlation coefficients (R) with the IAVs in monthly mean solar radiation  
 262 (SR) for each month in 1999-2021 and 1999-2017. In this analysis, the data for 2004 were not  
 263 included since the forest ecosystem around our site was disturbed by typhoons from June to  
 264 October. The correlations are also shown in Fig. S2. Significant positive correlations are found  
 265 for each month from July to September for 1999-2021 and 1999-2017, while significant  
 266 correlations are not found for June. With respect to August, the R values for 1999-2021 decrease  
 267 by almost 0.2, compared to those for the period 1999-2017.

268 Next, we carried out correlational analyses of the IAVs in NEP and GPP with LAI. In  
 269 addition to the analyses of the IAVs in monthly mean LAI for each month from June to  
 270 September with the IAVs of the monthly mean NEP and GPP for respective months, we also  
 271 conducted the same analysis with the IAVs of the annual NEP and GPP of the corresponding  
 272 year. In this analysis, the data for 2019 were excluded due to the problem with the PAR  
 273 measurement during the year, as mentioned above. The results are shown in Table 2 and Fig.  
 274 S3. The correlations of the IAVs in monthly mean LAI with those of monthly mean NEP and  
 275 GPP from June to September of 1999-2017 and for June, August and September of 1999-2021  
 276 are significantly positive for each month. The statistical significance for June-August of 1999-  
 277 2021 are less compared to those of 1999-2017. The IAVs in the monthly mean LAI for the  
 278 respective months of June to September also show significantly positive correlations with those  
 279 in the annual NEP and GPP, and each of the correlations shows larger significance in 1999-  
 280 2017 than in 1999-2021.

**Table 2.** Correlation coefficients (R) of IAV in monthly mean LAI for each of June, July, August and September with those in monthly mean NEP and GPP for the respective months and with those in annual NEP and GPP in the same year in 1999-2021 except for 2019 and in 1999-2017.

281

	June	July	August	September
Monthly NEP				
1999-2021	0.58***	0.31	0.44**	0.78****
1999-2017	0.79****	0.58***	0.64***	0.82****
Monthly GPP				
1999-2021	0.59***	0.30	0.45**	0.77****
1999-2017	0.77****	0.56**	0.63***	0.80****
Annual NEP				
1999-2021	0.36*	0.55***	0.61***	0.61***
1999-2017	0.66***	0.77****	0.83****	0.82****
Annual GPP				
1999-2021	0.46**	0.59***	0.64***	0.58***
1999-2017	0.72****	0.78****	0.84****	0.80****

Note: \*, \*\*, \*\*\* and \*\*\*\* represent statistical significance of correlations for  $0.1 < P \leq 0.05$ ,  $0.05 < P \leq 0.01$ ,  $0.01 < P \leq 0.001$  and  $P < 0.001$ , respectively.

282

#### 283 **4.2. Influence of IAV in NGP on those in annual NEP and GPP**

284 The IAV in the NGP can also contribute to the IAVs in the annual NEP and GPP. Earlier  
 285 occurrence of the NGS and/or later occurrence of the NGE can result in a longer NGP, and it  
 286 can cause increase in annual NEP. In Table 3, the R values of the IAVs in annual NEP and GPP  
 287 with those of the NGS and NGE and the length of the NGP of the respective years in 1999-2021  
 288 and 1999-2017 are shown. In the analysis, the data of 2004 are not included due to the above  
 289 mentioned reason. The correlations of IAVs in NGS, NGE and NGP with those in annual NEP  
 290 and GPP are also shown in Fig. S4. The IAVs in the annual NEP and GPP show significant  
 291 positive correlation with the IAV in NGP for both 1999-2021 and 1999-2017 though the  
 292 correlations are much more significant in 1999-2017 than in 1999-2021 periods. Significant  
 293 negative correlations of IAV in NGS with that in annual GPP for both periods and significant  
 294 positive correlations of IAV in NGE with those in annual NEP and GPP for 1999-2017 are also  
 295 shown.

**Table 3.** Correlation coefficient (R) of IAVs in NGS, NGE and NGP with those of annual NEP and GPP and environmental factors for 1999-2021 and 1999-2017.

296

	Parameter	R	
		1999-2021	1999-2017
NGS	Annual NEP	-0.34	-0.38
	Annual GPP	-0.45**	-0.46*
	T_spring	-0.75****	-0.81****
	LE <sub>LAI</sub>	0.83****	0.80****
	LE <sub>CET</sub>	0.81****	0.80****
NGE	Annual NEP	0.30	0.57**
	Annual GPP	0.20	0.46*
	SR_SEP	0.70****	0.68****
	LAI_SEP	0.38*	0.29
	LF <sub>LAI</sub>	0.58****	0.51**
	LF <sub>CET</sub>	0.30	0.24
NGP	Annual NEP	0.57****	0.75****
	Annual GPP	0.58****	0.72****
	T_spring	0.39*	0.40*
	SR_SEP	0.44**	0.56**
	LAI_SEP	0.45**	0.61****

Note: T\_spring is mean T from March to May. SR\_September and LAI\_September are monthly mean SR and LAI in September, respectively. The data of 2004 are excluded in this analysis. The data of LE<sub>LAI</sub>, LF<sub>LAI</sub> and LAI\_September for 2019 are also excluded in this analysis. \*, \*\*, \*\*\* and \*\*\*\* represent statistical significance of correlations for  $0.1 < P \leq 0.05$ ,  $0.05 < P \leq 0.01$ ,  $0.01 < P \leq 0.001$  and  $P < 0.001$ , respectively.

297

298 We then proceeded to examine the possible impacts of the plant phenological events such  
 299 as leaf expansion (LE) and leaf fall (LF) of canopy trees and environmental factors on NGS,  
 300 NGE and NGP. In this study, the first day of the year that LAI exceeded 50% of the average  
 301 value of LAI over DOY 180-240 (i.e., local summer) of the year, when the LAI values were  
 302 fairly stable and the maximum of the year appeared, was defined as an indicator (LE<sub>LAI</sub>) of the  
 303 occurrence of LE. Such simplified indicator allows us to examine the IAV in forest canopy  
 304 phenology and its impacts on CO<sub>2</sub> flux. Similarly, the first day of the year that LAI fell below  
 305 50% of the average value of the LAI over DOY 180-240 of the year was defined as an indicator  
 306 (LF<sub>LAI</sub>) of the occurrence of LF. Furthermore, we also calculated the occurrences of LE and LF  
 307 of canopy trees of each year using a degree-day model of vegetation phenology by Nagai et al.  
 308 (2021). In the model optimized to reproduce the phenology events at TKY, the LE date (LE<sub>CET</sub>)  
 309 was defined as the first day when the cumulative effect temperature (CET) was greater than

310 255.4°C. The  $CET_{st}$  was calculated with Eq. (9), where  $T_i$  is the daily mean air temperature (°C)  
 311 at 25-m height, and we set the start date to be January 1st and the threshold temperature for the  
 312 CET to be 2°C.

$$313 \quad CET_{st} = \sum_{i=January\ 1}^{LE_{CET}} \max(T_i - 2, 0), \quad (9)$$

314 The LF date ( $LF_{CET}$ ) was also defined as the first day when the CET was less than  $-375.1^\circ\text{C}$ .  
 315 The  $CET_{en}$  was calculated with Eq (10), where we set the start date to be August 1st and the  
 316 threshold temperature for the CET to be 18°C.

$$317 \quad CET_{en} = \sum_{i=August\ 1}^{LF_{CET}} \min(T_i - 18, 0), \quad (10)$$

318 Note that the occurrences of  $LE_{CET}$  and  $LF_{CET}$  are earlier and later than those of  $LE_{LAI}$  and  $LF_{LAI}$ ,  
 319 respectively since the  $LE_{CET}$  and the  $LF_{CET}$  are the parameters to estimate the start of leaf  
 320 expansion and the end of leaf fall, respectively (Nagai et al., 2013). Also, factors other than air  
 321 temperature such as impacts of disturbances of the forest ecosystem are not considered in the  
 322 model. The correlations of the IAVs in NGS, NGE and NGP with those in the  $LE_{CET}$  and the  
 323  $LF_{CET}$  were also examined. The IAVs in the occurrences of  $LE_{LAI}$ ,  $LF_{LAI}$ ,  $LE_{CET}$  and  $LF_{CET}$  thus  
 324 obtained along with those of NGS and NGE are shown in Fig. 5. As described above, the  
 325 occurrences of  $LE_{LAI}$  and  $LF_{CET}$  are later than those of  $LE_{CET}$  and  $LF_{LAI}$ , respectively. It can  
 326 also be seen in the figure that the occurrences of NGS and NGE are closer to those of  $LE_{CET}$   
 327 and  $LF_{LAI}$  than those of  $LE_{LAI}$  and  $LF_{CET}$ , respectively in most of the years during the 1999-  
 328 2021 period. In 2004 when the disturbances due to typhoons occurred, NGE occurred very  
 329 earlier than the other years.

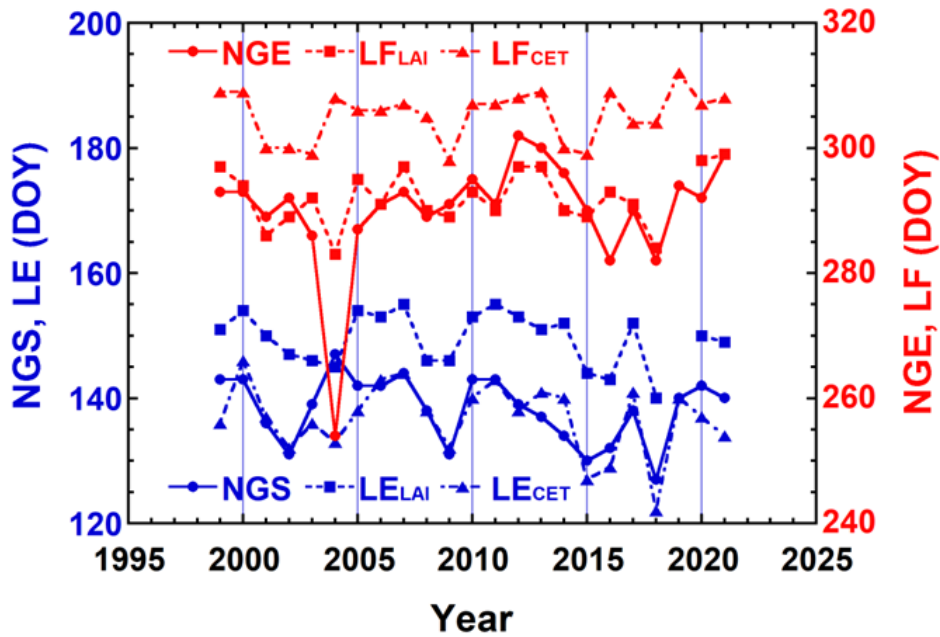


**Figure 5.** IAVs in occurrences of NGS, NGE,  $LE_{LAI}$ ,  $LF_{LAI}$ ,  $LE_{CET}$  and  $LF_{CET}$ .  $LE_{LAI}$  and  $LF_{LAI}$  for 2019 are not plotted because of no available LAI data.

330 Correlations of the IAV in NGS, NGE and NGP with those in environmental factors are  
331 also shown in Table 3 and Fig. S5. The IAV in the occurrence of NGS is significantly negatively  
332 and positively correlated with those in the mean air temperature from March to May (T\_spring)  
333 and the occurrences of LE (LE<sub>LAI</sub> and LE<sub>CET</sub>), respectively. Significantly positive correlations  
334 of the IAV in the occurrence of the NGE are also found with those in the occurrence of LF<sub>LAI</sub>  
335 and the monthly mean SR (SR\_SEP) and LAI (LAI\_SEP) in September though the correlations  
336 with LAI\_SEP for 1999-2017 and the occurrence of LF<sub>CET</sub> are not significant. With respect to  
337 the NGP, its IAV shows significantly positive correlations with those in T\_spring, SR\_SEP and  
338 LAI\_SEP.

339

#### 340 **4.3. Trends of annual carbon budget components and their environmental factors**

341 Figure 2 shows a linear increasing trend in the annual Rec during the period of 1994-2021  
342 ( $0.90 \pm 0.47$  ( $1\sigma$ )  $\text{gC m}^{-2} \text{yr}^{-1} \text{yr}^{-1}$ ,  $R = 0.35$ ,  $P < 0.1$ ) based on both the EC and AD data. This  
343 trend may be partly attributed to a significant increasing trend of annual mean air temperature  
344 observed at TKY during the period ( $+0.045 \pm 0.012$  ( $1\sigma$ )  $^{\circ}\text{C yr}^{-1}$ ,  $R = 0.59$ ,  $P < 0.01$ ). However,  
345 no significant linear trends were found in annual NEP and GPP IAVs over the same period.  
346 Also, no significant linear trends were found in IAVs of annual NEP, GPP and Rec for the EC  
347 observation period of 1999-2021. On the other hand, significantly increasing trends in annual  
348 NEP ( $31.9 \pm 4.5$  ( $1\sigma$ )  $\text{gC m}^{-2} \text{yr}^{-1} \text{yr}^{-1}$ ,  $R = 0.94$ ,  $P < 0.001$ ) and GPP ( $31.8 \pm 4.0$  ( $1\sigma$ )  $\text{gC m}^{-2}$   
349  $\text{yr}^{-1} \text{yr}^{-1}$ ,  $R = 0.94$ ,  $P < 0.001$ ) in 2004-2013 were found, while significantly decreasing trends  
350 were detected in annual NEP ( $-28.8 \pm 4.2$  ( $1\sigma$ )  $\text{gC m}^{-2} \text{yr}^{-1} \text{yr}^{-1}$ ,  $R = 0.93$ ,  $P < 0.001$ ) and in GPP  
351 ( $-27.4 \pm 5.2$  ( $1\sigma$ )  $\text{gC m}^{-2} \text{yr}^{-1} \text{yr}^{-1}$ ,  $R = 0.89$ ,  $P < 0.01$ ) for the period 2013-2021.

352 Figure 6 shows IAVs in the monthly mean NEP and GPP of each month from June to  
353 September, as well as NGS, NGE and NGP. The monthly mean NEP (Fig. 6a) and GPP (Fig.  
354 6b) values of June and from July to September show significantly increasing trends during  
355 2004-2016 and 2004-2013, respectively, while significantly decreasing trends are found from  
356 June to September in 2013-2021. Figure 6c shows a significant trend pointing to an ever earlier  
357 occurrence of NGS (2004-2018), as well as to an ever later occurrence of NGE (2005-2013).  
358 As a result, a significantly increasing trend of NGP is also seen (2005-2013). It is interesting to  
359 note that the NGE trend reverses from 2013 to 2018, indicating an earlier occurrence each year.

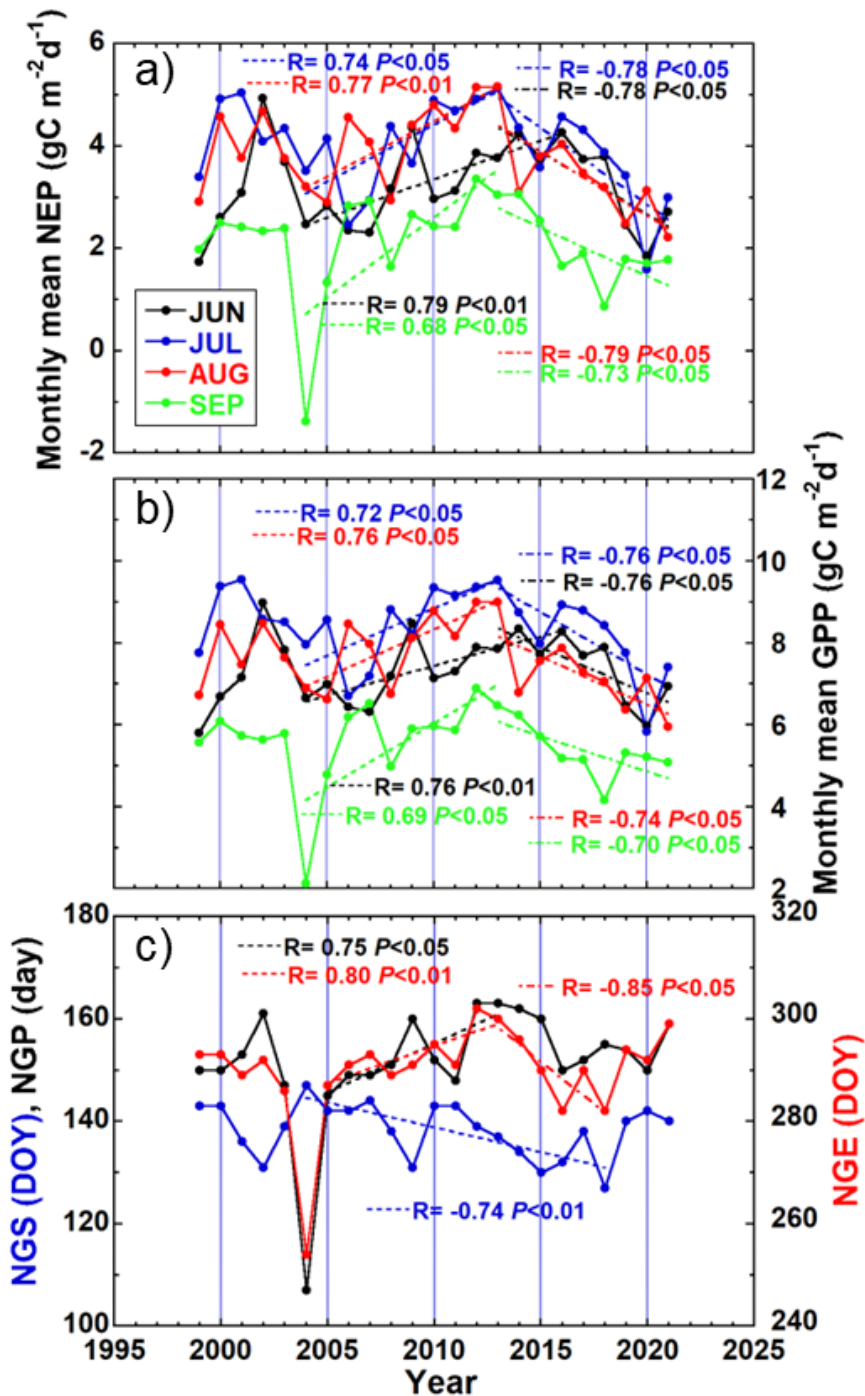


**Figure 6.** IAVs and significant trends of a) the monthly mean NEP, b) the monthly mean GPP of June-September, and c) the occurrences of the NGS (blue) and the NGE (red) and the length of the NGP (black).

360 Figure 7 shows IAVs in monthly mean LAI, SR and daytime (11:00-17:00 local time) vapor  
 361 pressure deficit (VPD) from June to September, together with spring (from March to May) and  
 362 August mean air temperatures. The LAI decreased from 2003 to 2004 due to the typhoons in  
 363 2004 (Fig. 7a). After this, while showing some fluctuations, the LAI gradually increased as the  
 364 forest canopy recovered, and showed significantly increasing trends for each month of July to

365 September in 2004-2013 and for June in 2004-2016; the significant increase in the NEP and  
 366 GPP trends were also observed for 2004-2013, as described above. During the period of 2013-  
 367 2021, when significant decrease in the NEP and GPP trends were observed, the mean LAI for  
 368 July and August maintained high values. The low LAI value in September 2018 was caused by  
 369 a typhoon; however, the September value showed a significantly decreasing trend for  
 370 September during 2013-2018.

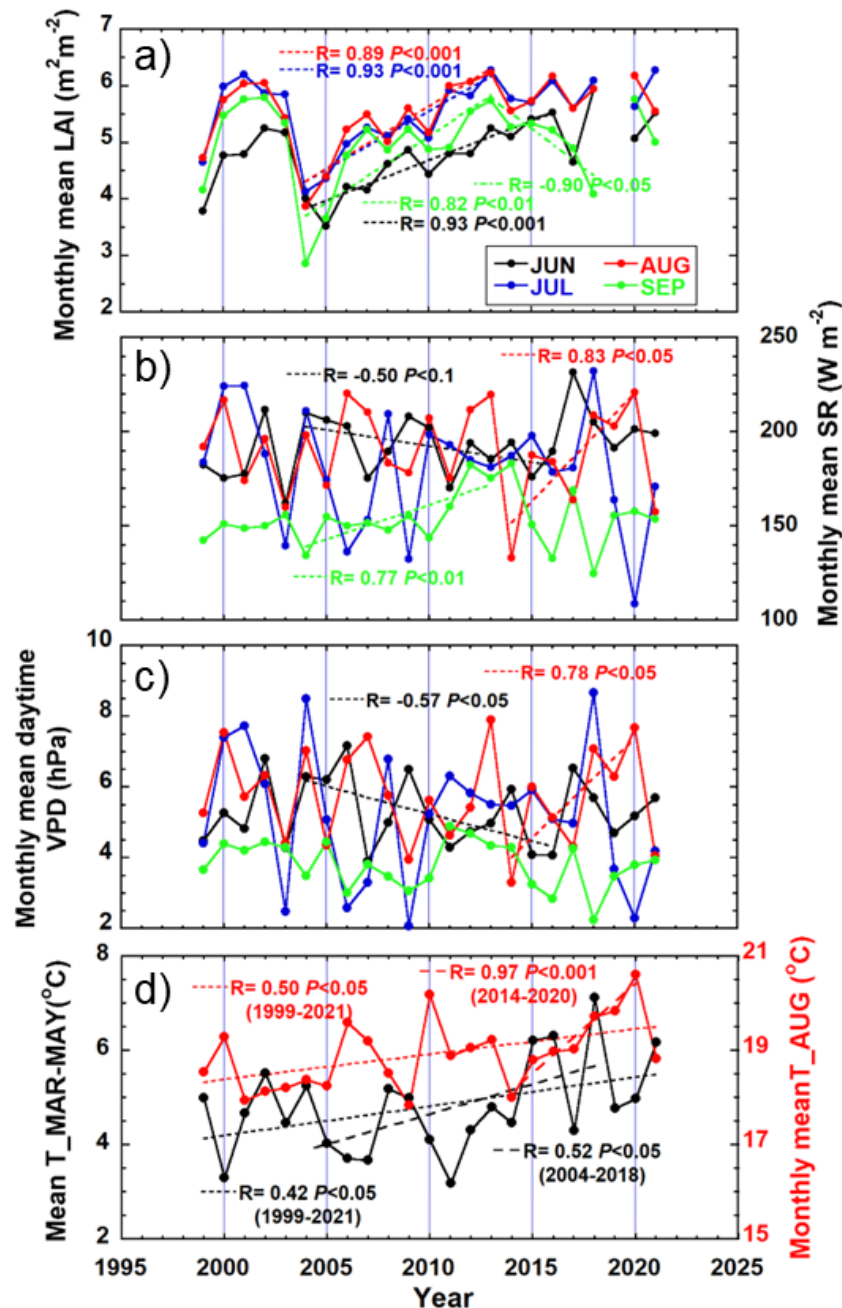


**Figure 7.** IAVs and significant trends in a) the monthly mean LAI, b) the monthly mean solar radiation, c) the monthly mean daytime (11:00-17:00) VPD of June-September, and d) the spring (from March to May) mean and the August monthly mean air temperatures.

371 The monthly mean SR in September and the mean air temperature in spring (from March  
372 to May) also showed significantly increasing trends in 2005-2013 and in 2004-2018 (also in  
373 1999-2021), respectively (Figs. 7b and d), while the decreasing trends of the monthly mean SR  
374 and daytime VPD in June were found in 2004-2016 (Figs. 7b and c). Using the F-test, the IAVs  
375 ( $1\sigma$ ) in the monthly mean SR were found to be significantly larger in 2014-2021 than in 2005-  
376 2013 for August ( $P < 0.01$ ) and for July and September ( $P < 0.05$ ) (Fig. 7b). The monthly mean  
377 air temperature in August also showed a significantly increasing trend in 1999-2021 (Fig. 7d)  
378 and a rapidly increasing trend especially in 2013-2020, accompanied by significantly increasing  
379 trends of the monthly mean SR and daytime VPD for the month (Figs. 7b and c).

380

## 381 **5. Discussion**

### 382 **5. 1. IAV in annual carbon budget**

383 Baldocchi et al. (2018) reported in their review paper that the average of the IAV ( $1\sigma$ ) in  
384 the annual NEE was close to  $100 \text{ gC m}^{-2} \text{ yr}^{-1}$  for long-term EC observations at temperate  
385 deciduous forest sites. There are various factors governing the IAV calculated from long-term  
386 observations (e.g., Froelich et al., 2015; Urbanski, et al., 2007). Among them, Baldocchi et al.  
387 (2018) identified the IAV in the length of the growing season to be a dominant factor affecting  
388 the IAV in annual NEP across much of the deciduous forests influenced by drastic changes in  
389 meteorological conditions that influence phenology of plant photosynthesis (e.g., Wilson et al.  
390 2000; Muraoka et al. 2010).

391 For the TKY deciduous forest site, the IAV ( $1\sigma$ ) in the annual NEP in 1999-2021 ( $83 \text{ gC}$   
392  $\text{m}^{-2} \text{ yr}^{-1}$ ) was found to be within range of the published results. The IAV in annual NEP largely  
393 depended on the IAV in annual GPP (Fig. 2). Furthermore, the concept developed from Fig. 3  
394 is supported by the significantly positive correlations of the IAVs in annual NEP and GPP with  
395 the IAVs in monthly mean NEP and GPP of each month from June to September (Subsection  
396 4.1, Fig. 4) and the length of NGP (Subsection 4.2, Table 3). The significantly positive  
397 correlations with the IAVs in the monthly mean LAI of each month from June to September  
398 also suggested that the IAV in LAI during the growing season also had much influence on the  
399 IAVs in annual NEP and GPP (Subsection 4.1, Table 2). Although some significant correlations  
400 of the IAVs in NGS and NGE were found with those in annual NEP and GPP, each of the IAVs  
401 in NGS and NGE did not so strongly govern those in annual NEP and GPP as that in NGP.

402 With respect to the IAVs in the monthly mean NEP and GPP from June to September, it  
403 was found from significant correlations for most of these months (Tables 1 and 2) that the IAVs  
404 in the monthly mean SR and LAI from summer to early fall were likely to be important factors  
405 governing the  $\text{CO}_2$  uptake variability by the forest ecosystem for the corresponding months.  
406 However, for the monthly mean SR of June, the correlations were not very significant with the  
407 monthly NEP and GPP. In June, LAI rapidly increases and does not yet reach the annual  
408 maximum value as shown in Fig. S1. The coefficient of variation (CV; the ratio of the standard

409 deviation to the average) of the monthly mean SR for June is smaller than those for July, August  
410 and September (Fig. 8b). This may result in the relatively weak correlations of the IAVs in the  
411 monthly mean NEP and GPP with that in the monthly mean SR for June (Table 1).

412 Significance of the correlations of the IAVs in annual NEP and GPP with those in monthly  
413 mean LAI of each month from June to September (Table 2), NGP and NGE (Table 3) were  
414 largely diminished for 1999-2021 compared to 1999-2017. Also, significance of the correlations  
415 of the IAVs in corresponding monthly mean NEP and GPP with those in monthly mean SR in  
416 August (Table 1) and LAI for each month from June to August (Table 2) were even lower for  
417 1999-2021 than for 1999-2017. These will be discussed in Subsection 5.2.

418 The significant correlations shown in Table 3 indicate that the IAVs in the mean air  
419 temperature in spring (March-May) and the occurrence of  $LE_{CET}$  are dominant environmental  
420 drivers for the IAV in NGS; the IAV in  $LE_{LAI}$  was not considered to be the driver since the  
421 occurrence of NGS was earlier than that of  $LE_{LAI}$  in most of the years for 1999-2021 (Fig. 5),  
422 though a significant correlation in IAV was also shown between NGS and that of  $LE_{LAI}$ . Warmer  
423 spring leads to an earlier LE of canopy trees and an earlier start of enhancement of  
424 photosynthetic activities including understory dwarf bamboo, resulting in an earlier occurrence  
425 of NGS. On the other hand, since higher SR and LAI in early fall (September) and later  
426 occurrence of  $LF_{LAI}$  maintain higher photosynthetic activities of the ecosystem in the growing  
427 season, these factors lead to a later occurrence of NGE. Since photosynthesis was fairly  
428 suppressed around the time of  $LF_{CET}$ , the correlation is considered to be weak. Thus, warmer  
429 spring and higher SR and LAI in early fall (September) expanded the length of NGP, resulting  
430 in significant correlations of the IAV in NGP with these factors.

431 Saigusa et al. (2005) demonstrated that the IAV in annual NEP was positively correlated  
432 with the IAV in monthly mean air temperature in April in 1994-2002 at TKY, suggesting that a  
433 warmer spring causes earlier LE, resulting in increased annual NEP. However, no significant  
434 correlation ( $R = 0.04$ ) was found in this study using a longer dataset of 1999-2021, though the  
435 IAV in spring mean air temperature was indirectly correlated with that in the annual NEP via  
436 significant correlation with the IAVs in the NGS and NGP. However, a significant positive  
437 correlation of the IAV in annual NEP was found with that in monthly mean SR in September  
438 ( $R = 0.46$ ,  $P < 0.05$  for 1999-2021 and  $R = 0.59$ ,  $P < 0.01$  for 1999-2017) from our long-term  
439 data (Figs. 2, 7 and S6). The result was consistent with the fact that the IAV in monthly mean  
440 SR in September was significantly positive correlated with those in monthly mean NEP in  
441 September and NGP, each of which showed a significantly positive correlation with that of  
442 annual NEP, as described in Subsections 4.1 and 4.2. Different results between our study and  
443 Saigusa et al. (2005) highlight the possibility that the degree of importance of identified  
444 ecosystem processes contributing to the IAV in the annual carbon budget can be a function of  
445 the length and data period of analysis. Therefore, it is important to identify any “unusual”  
446 environmental event in an analysis, particularly for an analysis of a short dataset.

## 447 **5.2. Trend of annual carbon budget**

448 An increasing trend of annual NEP has been observed at some forest sites (e.g., Urbanski  
449 et al., 2007; Froelich et al., 2015). For the TKY site, no significant trend of annual NEP was  
450 detected over the observed period. However, significant increasing trends were observed for  
451 annual NEP and GPP and monthly mean NEP and GPP of each month from July to September  
452 for 2004-2013 and June monthly mean NEP and GPP for 2004-2016, while significant  
453 decreasing trends of annual NEP and GPP and monthly mean NEP and GPP of each month from  
454 June to September were detected for 2013-2021 (Figs. 2, 7a and b; subsection 4.3). From  
455 comparative analyses (Figs. 7 and 8), the following observations can be drawn: (1) The above-  
456 mentioned increasing trends nearly synchronized with the increasing trend of LAI associated  
457 with the recovery from typhoon strikes in 2004. In addition to this, the increasing trends were  
458 also probably influenced by the NGP trend related to increasing trends of mean air temperature  
459 in spring (March-May) and monthly mean SR in September; they lead to a significant trend  
460 towards earlier occurrence of NGS and a delayed trend of NGE, respectively, which are  
461 consistent with the relationship of these meteorological parameters with NGS, NGE and NGP  
462 described in Subsection 4.2. (2) Although what factors caused the latter decreasing trends was  
463 not so clearly identified, the decreasing trends may be partly attributed to a significant trend  
464 towards earlier occurrence of NGE and a significantly decreasing trend of monthly mean LAI  
465 in September in 2013-2018 and fairly low SR observed in some months from summer to early  
466 fall for 2014-2020 such as in August 2014, September 2018 and July 2020 (significant larger  
467 IAV in SR in 2014-2021 than in 2005-2013 as described above).

468 Since the variability patterns of the monthly mean NEP and GPP were very similar, we  
469 further investigated the decreasing trends of the monthly mean GPP for 2013-2021. For the  
470 analysis, we simply obtained the following linear functions of the observed monthly mean SR  
471 ( $x$ ) and LAI ( $y$ ) which simulate the monthly mean GPP ( $z$ ) for each month from June to  
472 September using a multiple regression analysis for the observed data in 1999-2013 when the  
473 decreasing trends had not yet appeared:

$$474 \quad z = a_i + b_i \cdot x + c_i \cdot y \quad , (11)$$

475 where  $a$ ,  $b$  and  $c$  are constants and the subscript  $i$  denotes each month from June to September.  
476 The reason why Eq. 11 is a function of monthly mean SR and LAI is that the IAVs in monthly  
477 mean GPP were highly correlated with the IAVs in these parameters in many of the months, as  
478 shown in Tables 1 and 2. We simulated the monthly mean GPP of each of the months from 1999  
479 to 2021 except for 2019 (because of no available LAI data), and compared with the observed  
480 GPP. The result is given in Fig. 8. Since RMSE values of the simulation for June, July, August  
481 and September of 1999-2017 (0.39, 0.51, 0.38 and 0.55 gC m<sup>-2</sup> yr<sup>-1</sup>, respectively) were close to  
482 those of 1999-2013 (0.37, 0.50, 0.39 and 0.57 gC m<sup>-2</sup> yr<sup>-1</sup>, respectively), the relationship  
483 obtained from the 1999-2013 data are considered to be applicable up to 2017. However, the  
484 observed GPP values were noticeably smaller than the simulated values from 2018 to 2021,

485 especially for June to August. The result suggests that the prior relationship between the IAV in  
486 GPP and its causative factors changed after 2017. This result may also be related to the facts  
487 that the significance of some of the correlations for 1999-2021 shown in Tables 1-3 was largely  
488 diminished compared to 1999-2017, as described in Subsection 5.1. High monthly mean  
489 temperatures in July 2018 and August of 2018-2020 (the highest monthly average temperatures  
490 in the top six for 1994-2021 were observed in these months), high monthly mean daytime VPD  
491 during the same months and the record low monthly SR and high monthly precipitation (>1000  
492 mm) in July 2020 were observed. The record-breaking heatwave also dominated over Japan  
493 and Korea from mid-July to early August 2018, and it has been pointed out that it may have  
494 decreased GPP in the area during the period (Yamamoto et al., 2023). The area around TKY has  
495 humid and cool summer due to Asian Monsoon and high altitude. Therefore, a decrease in GPP  
496 due to hot and dry weather had barely been observed at TKY. However, such recently frequent  
497 occurrences of extreme weather may suppress photosynthetic activities and have altered the  
498 past relationship. To clarify the mechanism of the recent decreasing trends, further analyses and  
499 data accumulation are necessary, which probably contribute to better understanding of the  
500 impacts of climate change on the forest ecosystem at TKY.

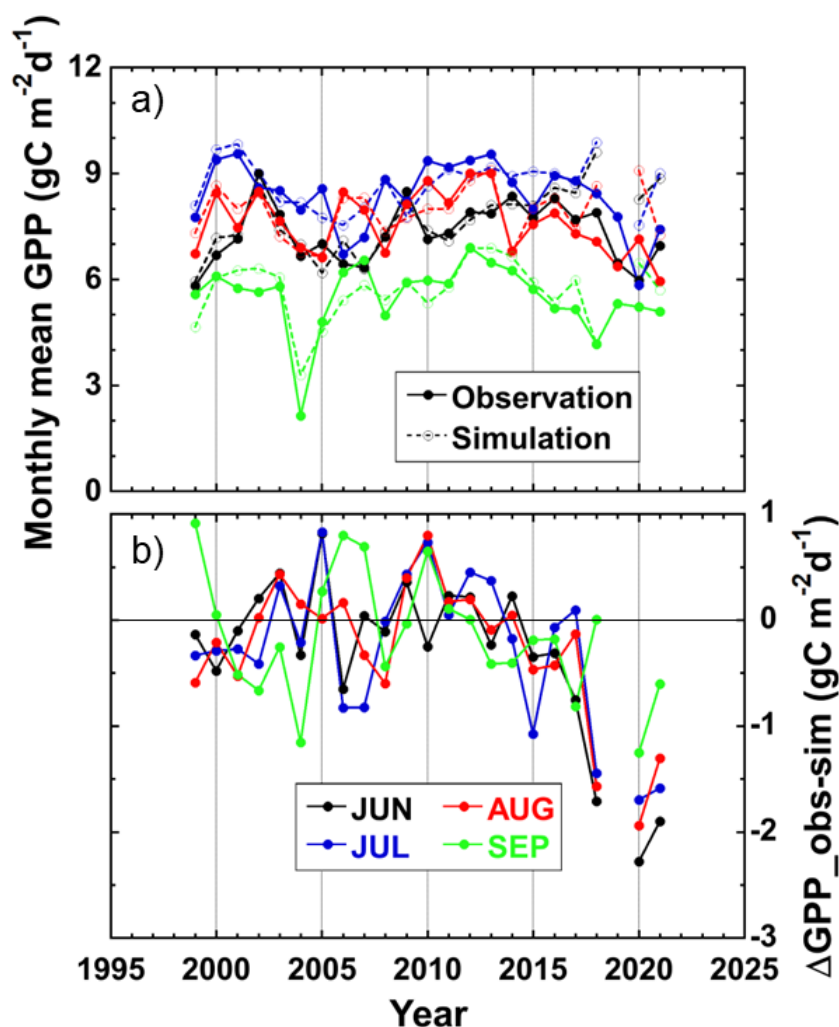


**Figure 8.** a) Comparison of IAVs in the monthly mean GPP of June-September between the observation and the simulation based on a multiple regression analysis, and b) IAVs in difference of the monthly mean GPP between the observation and the simulation.

501

### 502 **5.3. Influence of interseasonal factors on IAV in carbon budget components**

503 We further examined relationships between the variations in some of the factors, especially  
 504 between those in phenomena occurring in different seasons, and their influences on the IAV in  
 505 the carbon budget components at TKY. A significantly positive correlation was found between  
 506 IAVs of NGS and NGE in 1999-2021 (Table 4, Fig. S7a), which indicates that NGE tends to  
 507 occur early in the same year of early occurrence of NGS and vice versa. It is interesting to note  
 508 that such a significant correlation of the IAVs can be seen in different seasons. As described in  
 509 Subsections 4.2 and 5.1, the IAVs in NGS and NGE showed significantly positive correlations  
 510 with those in LE ( $LE_{LAI}$  and  $LE_{CET}$ ) and  $LF_{LAI}$ , respectively, suggesting that the IAVs in NGS  
 511 and NGE are influenced by variability in the forest canopy phenology. The IAVs in  $LE_{LAI}$  and  
 512  $LE_{CET}$  were also positively correlated with those in  $LF_{LAI}$  and  $LF_{CET}$ , respectively (Table 4, Figs.

513 S7b and c), showing that LF tends to occur early in the same year of early occurrence of LE  
 514 and vice versa. Therefore, the positive correlation between NGS and NGE observed at TKY  
 515 may be attributed to such interseasonal-phenological characteristics at the site. Some recent  
 516 studies also found that earlier/later LF is associated with earlier/later LE at some temperate  
 517 deciduous forests, and pointed out that winter-spring warming due to climate change will not  
 518 always lead to extension of the growing season into the future (Fu et al., 2014; Keenan &  
 519 Richardson, 2015; Piao et al., 2019b; Zani et al., 2020).  
 520

**Table 4.** Correlation coefficients (R) of IAVs between interseasonal parameters for each period.

Interseasonal parameter	Period	R
NGS vs. NGE	1999-2021	0.37*
LE <sub>LAI</sub> vs. LF <sub>LAI</sub>	1999-2021	0.50**
LE <sub>CET</sub> vs. LF <sub>CET</sub>	1999-2021	0.39*
T_Spring vs. SR_September	1994-2021	-0.33*

Note: T\_Spring and SR\_September represent mean T from March to May and monthly mean SR in September, respectively. The data for 2004 are excluded for the analysis of NGS vs. NGE, LE<sub>LAI</sub> vs. LF<sub>LAI</sub> and LE<sub>CET</sub> vs. LF<sub>CET</sub>. The data for 2019 are also excluded for the analysis of LE<sub>LAI</sub> vs. LF<sub>LAI</sub>. \* and \*\* represent statistical significance of correlations for  $0.1 < P \leq 0.05$  and  $0.05 < P \leq 0.01$ , respectively.

521 On the other hand, significant correlations in the IAV were also found between  
 522 meteorological parameters observed in different seasons at TKY. A negative correlation of the  
 523 IAV in the mean air temperature in spring (March-May) was seen with the IAV in the monthly  
 524 mean SR in September (Table 4, Fig. S7d). The relationships of the IAVs in these  
 525 meteorological parameters with those in NGS, NGE and NGP were described in Subsection 4.2.  
 526 From these relationships, it is suggested that early/late occurrence of NGS and long/short NGP  
 527 related to high/low temperature in spring tend to be accompanied with early/late occurrence of  
 528 NGE and short/long NGP related to low/high SR in early fall in the same year. Therefore, the  
 529 positive correlation between NGS and NGE observed at TKY may also be influenced by such  
 530 an interseasonal relationship of the meteorological parameters at the site. Whichever process  
 531 caused the positive correlation between NGS and NGE, these opposite effects on the length of  
 532 NGP of the year partly offset each other and the difference between the two effects may cause  
 533 the IAV in NGP. Such a mechanism of the IAV in NGP probably affects those in annual NEP  
 534 and GPP at TKY.

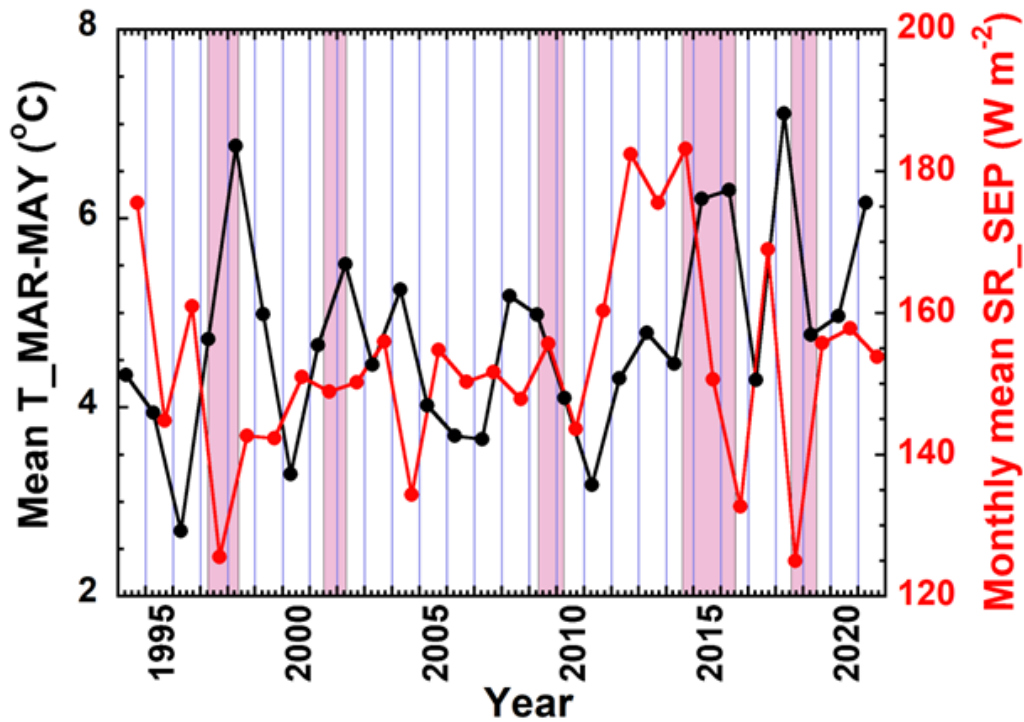


**Figure 9.** IAVs in mean air temperature from March to May (black) and solar radiation in September (red). Pink-shades represent El Niño periods.

535

536 High temperature anomaly from winter to spring and low temperature and low SR anomaly  
 537 from summer to fall tend to be observed during the El Niño period in Japan (Saigusa et al.,  
 538 2005; [https://ds.data.jma.go.jp/tcc/tcc/products/climate/ENSO/el\\_nino.html](https://ds.data.jma.go.jp/tcc/tcc/products/climate/ENSO/el_nino.html)). Figure 9 shows  
 539 the IAVs in the mean air temperature in spring and the monthly mean SR in September observed  
 540 at TKY, along with the recent El Niño periods  
 541 ([https://www.data.jma.go.jp/tcc/tcc/products/el\\_nino/ensoevents.html](https://www.data.jma.go.jp/tcc/tcc/products/el_nino/ensoevents.html)). The IAVs in these  
 542 parameters seem to reflect such meteorological characteristics in Japan during the El Niño  
 543 period, except for a few cases. Therefore, the above-mentioned interseasonal relationship of the  
 544 meteorological parameters observed at TKY is considered to be likely influenced by the ENSO  
 545 events. Using an earlier observational data, Saigusa et al. (2005) pointed out the influence of El  
 546 Niño on the canopy phenology and the carbon budget of the forest ecosystem at TKY. The  
 547 present study also suggests that the IAVs in the phenology and the carbon budget obtained from  
 548 our long-term observation were influenced by ENSO events. Many studies reported that hot  
 549 and dry weather conditions associated with El Niño events often cause drought and forest fires  
 550 in wide areas such as Southeast Asia and South America, leading to enhancement of CO<sub>2</sub> release  
 551 from global terrestrial biosphere (e.g., IPCC, 2021; Rödenbeck et al., 2018; Liu et al., 2017;  
 552 Goto et al., 2017). However, this is not the case for TKY, since different weather conditions  
 553 such as wet and cloudy summer-early fall and warm winter-spring tend to be observed around  
 554 our site during the El Niño period.

555

## 556 **6. Summary**

557 We initiated a long-term measurement of CO<sub>2</sub> flux between the atmosphere and the forest  
558 ecosystem in September of 1993 at TKY in a cool-temperate deciduous forest in central Japan.  
559 In this paper, we reanalyzed the long-term data mainly obtained from the EC measurements  
560 obtained during 1999-2021. The IAVs and the trends of annual carbon budget components were  
561 examined, and then their environmental factors were investigated.

562 The main results obtained from the analyses are as follows:

563 (1) The annual NEP, GPP and Rec (mean  $\pm 1\sigma$ ) for the EC measurement period were  $265 \pm 86$ ,  
564  $1066 \pm 91$ , and  $801 \pm 21$  gC m<sup>-2</sup> yr<sup>-1</sup>, respectively. The IAV in the annual NEP strongly depended  
565 on the IAV of annual GPP.

566 (2) Based on the significant correlations with the IAVs in monthly mean NEP, GPP and LAI for  
567 each month from June to September, the IAVs in annual NEP and GPP largely depended on  
568 those in NEP, GPP and LAI from summer to early fall. The IAVs in the monthly mean NEP and  
569 GPP were attributed to those in the monthly mean SR from July to September and those in the  
570 monthly mean LAI from June to September for the respective months.

571 (3) The IAVs in the annual NEP and GPP were governed by the IAV in NGS. Early/late  
572 occurrence of NGS was attributed to warm/cold spring and early/late occurrence of LE<sub>CET</sub>,  
573 while late/early occurrence of NGE was associated with high/low monthly mean SR in  
574 September and late/early LE<sub>LAI</sub>. Early NGS and/or late NGE led to long NGP.

575 (4) Significant increasing and decreasing trends of annual NEP and GPP were detected in 2004-  
576 2013 and 2013-2021, respectively. The former increasing trends were highly linked to recovery  
577 from the ecosystem disturbances due to typhoon strikes in 2004, and partly related to trends of  
578 some meteorological parameters. On the other hand, the cause of the latter decreasing trends  
579 was not clearly identified though the decreasing trend of the monthly mean LAI in September  
580 and the trend towards earlier occurrence of NGE for 2013-2018 may partly be related to them.

581 (5) The above-mentioned decreasing trends of annual NEP and GPP and the noticeably  
582 diminished significance seen in the correlations of the IAVs in carbon budget components with  
583 those in some environmental factors for 1999-2021 compared to 1999-2017 may have been  
584 influenced by the recent extreme weather conditions, such as high temperatures in August for  
585 2018-2020 and the record high monthly precipitation and low monthly SR in July 2020.

586 (6) Some intercorrelations of IAV between the events occurring in different seasons, such as the  
587 occurrences of NGS and NGE and the occurrences of LE and LF, were found. It was suggested  
588 that they may be attributed not only to some biological functions but also to meteorological  
589 parameters associated with ENSO events, which could have influence on annual carbon budget  
590 at TKY.

591 Some of the results obtained from the long-term measurement were found to be different  
592 from those shown in the previous studies that were based on shorter observation. Also, decadal

593 scale phenomena such as increasing and decreasing trends of annual NEP and GPP could not  
594 be detected without the long-term observation. Therefore, long-term observations are very  
595 important for better understanding of the carbon cycle in forest ecosystems. Collaboration with  
596 studies using various approaches such as biometric measurements (Ohtsuka et al., 2009) and  
597 model simulations (Ito et al., 2010b; Higuchi et al., 2005) should be further developed. Such  
598 multidisciplinary studies based on long-term observations are essential to precisely predict  
599 responses of the terrestrial biosphere to climate change.

600

## 601 **Acknowledgements**

602 We would like to thank N. Nishimura, H. Koizumi, T. Akiyama, I. Tamagawa, K.  
603 Kurumado, S. Yoshitake, K. Suzuki, H. Hiratsuka, and members of the River Basin Research  
604 Center of Gifu University for their cooperation. We are also very grateful to K. Muto, H. Yatabe  
605 and Y. Takeda of National Institute of Advanced Industrial Science and Technology and A.  
606 Kudo and C. Abe of Japan ANS Co. Ltd. for their support to observation and data analyses.  
607 This study was partly supported by the JSPS KAKENHI (Grant Numbers JP24241008,  
608 JP24310017, JP15H02814, JP26241005, JP18H03365, JP19H03301, JP19H01975,  
609 JP21H05316, JP21H05312, JP22H00564 and JP22H05006) and the Global Environment  
610 Research Coordination System from the Ministry of the Environment, Japan (Grant Numbers  
611 MAFF0751, MAFF1251, MAFF2254), the Global Environment Research Fund of the Ministry  
612 of the Environment, Japan (S-1: Integrated Study for Terrestrial Carbon Management of Asia  
613 in the 21st Century Based on Scientific Advancement).

614

## 615 **Data Availability Statement**

616 The dataset of the carbon budget at TKY presented in the manuscript has been made  
617 publically available at <https://doi.org/10.5281/zenodo.8300684>.

618

## 619 **References**

- 620 Baldocchi, D., Falge, E., Gu, L., Olson, R., Hollinger, D., Running, S., et al. (2001). FLUXNET:  
621 A new tool to study the temporal and spatial variability of ecosystem-scale carbon dioxide,  
622 water vapor, and energy flux densities. *Bull. Amer. Meteorol. Soc.*, 82, 2415-2434,  
623 [https://doi.org/10.1175/1520-0477\(2001\)082<2415:FANTTS>2.3.CO;2](https://doi.org/10.1175/1520-0477(2001)082<2415:FANTTS>2.3.CO;2).
- 624 Baldocchi, D., Housen, C., & Reichstein, M. (2018). Inter-annual variability of net and gross  
625 ecosystem carbon fluxes: A review. *Agric. For. Meteorol.*, 249, 520-533,  
626 <https://doi.org/10.1016/j.agrformet.2017.05.015>.
- 627 Friedlingstein, P., O'Sullivan, M., Jones, M. W., Andrew, R. M., Gregor, L., Hauck, J., et al.,  
628 (2022). Global Carbon Budget 2022. *Earth Syst. Sci. Data*, 14, 4811-4900,  
629 <https://doi.org/10.5194/essd-14-4811-2022>.

630 Froelicha, N., Croft, H., Chen, J. M., Gonsamo, A., & Staebler, R. M. (2015). Trends of carbon  
631 fluxes and climate over a mixed temperate–boreal transition forest in southern Ontario,  
632 Canada. *Agric. For. Meteorol.*, 211-212, 72-84,  
633 <https://doi.org/10.1016/j.agrformet.2015.05.009>.

634 Fu, Y. S. H., Campioli, M., Vitasse, Y., Boeck, H. J. D., Berge, J. V. d., AbdElgawad, H., et al.  
635 (2014). Variation in leaf flushing date influences autumnal senescence and next year’s  
636 flushing date in two temperate tree species. *Proc. Natl. Acad. Sci.*, 111, 7355–7360,  
637 <https://doi.org/10.1073/pnas.1321727111>.

638 Goto, D., Morimoto, S., Ishidoya, S., Aoki, S., & Nakazawa, T. (2017). Terrestrial biospheric  
639 and oceanic CO<sub>2</sub> uptakes estimated from long-term measurements of atmospheric CO<sub>2</sub> mole  
640 fraction,  $\delta^{13}\text{C}$ , and  $\delta(\text{O}_2/\text{N}_2)$  at Ny-Ålesund, Svalbard. *J. Geophys. Res. Biogeosci.*, 122,  
641 1192-1202, <https://doi.org/10.1002/2017JG003845>.

642 Higuchi, K., Shashkov, A., Chan, D., Saigusa, N., Murayama, S., Yamamoto, S., et al. (2005).  
643 Simulations of seasonal and inter-annual variability of gross primary productivity at  
644 Takayama with BEPS ecosystem model. *Agri. For. Meteorol.*, 134, 143–150,  
645 <https://doi.org/10.1016/j.agrformet.2005.08.018>.

646 IPCC (2021). *Climate Change 2021: The Physical Science Basis. Contribution of Working*  
647 *Group I to the Sixth Assessment Report of the Intergovernmental Panel on Climate Change.*  
648 V. Masson-Delmotte, P. Zhai, A. Pirani, S.L. Connors, C. Péan, S. Berger, N. Caud, Y. Chen,  
649 L. Goldfarb, M.I. Gomis, M. Huang, K. Leitzell, E. Lonnoy, J.B.R. Matthews, T.K. Maycock,  
650 T. Waterfield, O. Yelekçi, R. Yu, & B. Zhou (eds.), 2391 pp., Cambridge University Press,  
651 Cambridge, UK and New York, USA, <https://doi.org/10.1017/9781009157896>.

652 Ishidoya, S., Murayama, S., Kondo, H., Saigusa, N., Kishimoto-Mo, A. W., & Yamamoto, S.  
653 (2015). Observation of O<sub>2</sub>:CO<sub>2</sub> exchange ratio for net turbulent fluxes and its application to  
654 forest carbon cycles. *Ecol. Res.*, 30, 225–234, <https://doi.org/10.1007/s11284-014-1241-3>.

655 Ito, A. (2010a). Evaluation of the impacts of defoliation by tropical cyclones on a Japanese  
656 forest’s carbon budget using flux data and a process-based model. *J. Geophys. Res.*, 115,  
657 G04013, <https://doi.org/10.1029/2010JG001314>.

658 Ito, A. (2010b). Changing ecophysiological processes and carbon budget in East Asian  
659 ecosystems under near-future changes in climate: implications for long-term monitoring  
660 from a process-based model. *J. Plant Res.*, 123, 577–588, [https://doi.org/10.1007/s10265-](https://doi.org/10.1007/s10265-009-0305-x)  
661 [009-0305-x](https://doi.org/10.1007/s10265-009-0305-x).

662 Ito, A., Saitoh, T. M., & Sasai, T. (2015). Synergies between observational and modeling studies  
663 at the Takayama site: toward a better understanding of processes in terrestrial ecosystems.  
664 *Ecol. Res.*, 30, 201–210, <https://doi.org/10.1007/s11284-014-1205-7>.

665 Keenan, T. F., & Richardson, A. D. (2015). The timing of autumn senescence is affected by the  
666 time of spring phenology: Implications for predictive models. *Global Change Biol.*, 21,  
667 2634–2641, <https://doi.org/10.1111/gcb.12890>.

668 Kondo, H., Saigusa, N., Murayama, S., Yamamoto, S., & Kannari, A. (2001). A numerical  
669 simulation of the daily variation of CO<sub>2</sub> in the central part of Japan summer case. *J. Meteorol.*  
670 *Soc. Jpn.*, 79, 11–21, <https://doi.org/10.2151/jmsj.79.11>.

671 Liu, J., Bowman, K. W., Schimel, D. S., Parazoo, N. C., Jiang, Z., Lee, M., et al. (2017).  
672 Contrasting carbon cycle responses of the tropical continents to the 2015–2016 El Niño.  
673 *Science*, 358, eaam5690, <https://doi.org/10.1126/science.aam5690>.

674 Muraoka, H., & Koizumi, H. (2005). Photosynthetic and structural characteristics of canopy  
675 and shrub trees in a cool-temperate deciduous broadleaved forest: Implication to the  
676 ecosystem carbon gain. *Agric. For. Meteorol.*, 134, 39–59.  
677 <https://doi.org/10.1016/j.agrformet.2005.08.013>.

678 Muraoka, H., Saigusa, N., Nasahara, K. N., Noda, H., Yoshino, J., Saitoh, T. M., et al. (2010).  
679 Effects of seasonal and interannual variations in leaf photosynthesis and canopy leaf area  
680 index on gross primary production of a cool-temperate deciduous broadleaf forest in  
681 Takayama, Japan. *J. Plant Res.*, 123, 563–576, <https://doi.org/10.1007/s10265-009-0270-4>.

682 Muraoka, H., Saitoh, T. M., & Nagai, S. (2015). Long-term and interdisciplinary research on  
683 forest ecosystem functions: challenges at Takayama site since 1993. *Ecol. Res.*, 30, 197–200,  
684 <https://doi.org/10.1007/s11284-015-1251-9>.

685 Murayama, S., Saigusa, N., Chan, D., Yamamoto, S., Kondo, H., & Eguchi, Y. (2003). Temporal  
686 variations of atmospheric CO<sub>2</sub> concentration in a temperate deciduous forest in central Japan.  
687 *Tellus, Ser. B*, 55, 232–243, <https://doi.org/10.1034/j.1600-0889.2003.00061.x>.

688 Murayama, S., Takamura, C., Yamamoto, S., Saigusa, N., Morimoto, S., Kondo, H., et al. (2010).  
689 Seasonal variations of atmospheric CO<sub>2</sub>, δ<sup>13</sup>C, and δ<sup>18</sup>O at a cool temperate deciduous forest  
690 in Japan: Influence of Asian monsoon. *J. Geophys. Res.*, 115, D17304,  
691 <https://doi.org/10.1029/2009JD013626>.

692 Musavi, T., Migliavacca, M., Reichstein, M., Kattge, J., Wirth, C., Black, T. A., et al. (2017).  
693 Stand age and species richness dampen interannual variation of ecosystem-level  
694 photosynthetic capacity. *Nature Ecol. Evol.*, 1, 0048, <https://doi.org/10.1038/s41559-016-0048-0048>.

696 Nagai, S., Saitoh, T. M., & Nasahara, K. N. (2021). How did the characteristics of the growing  
697 season change during the past 100 years at a steep river basin in Japan? *PLoS ONE*, 16,  
698 e0255078, <https://doi.org/10.1371/journal.pone.0255078>.

699 Nagai, S., Saitoh, T. M., Kurumado, K., Tamagawa, I., Kobayashi, H., Inoue, T., et al. (2013).  
700 Detection of bio-meteorological year-to-year variation by using digital canopy surface  
701 images of a deciduous broad-leaved forest. *SOLA*, 9, 106–110,  
702 <https://doi.org/10.2151/sola.2013-024>.

703 Nakazawa, T., Ishizawa, M., Higuchi, K., & Trivett, N. B. A. (1997). Two curve fitting method  
704 applied to CO<sub>2</sub> flask data. *Environmetrics*, 8, 889–906, [https://doi.org/10.1002/\(SICI\)1099-095X\(199705\)8:3<197::AID-ENV248>3.0.CO;2-C](https://doi.org/10.1002/(SICI)1099-095X(199705)8:3<197::AID-ENV248>3.0.CO;2-C).

706 Nasahara, K. N., Muraoka, H., Nagai, S., & Mikami, H. (2008). Vertical integration of leaf area  
707 index in a Japanese deciduous broad-leaved forest. *Agric. For. Meteorol.*, 148, 1136-1146,  
708 <https://doi.org/10.1016/j.agrformet.2008.02.011>.

709 Ohtsuka, T., Mo, W., Satomura, T., Inatomi, M., & Koizumi, H. (2007). Biometric based carbon  
710 flux measurements and net ecosystem production (NEP) in a temperate deciduous broad-  
711 leaved forest beneath a flux tower. *Ecosystems*, 10, 324-334,  
712 <https://doi.org/10.1007/s10021-007-9017-z>.

713 Ohtsuka, T., Saigusa, N., & Koizumi, H. (2009). On linking multiyear biometric measurements  
714 of tree growth with eddy covariance-based net ecosystem production. *Global Change Biol.*,  
715 15, 1015-1024, <https://doi.org/10.1111/j.1365-2486.2008.01800.x>.

716 Piao, S., Qiang, L., Chen, A., Janssens, I. A., Fu, Y., Dai, J., et al. (2019b). Plant phenology and  
717 global climate change: Current progresses and challenges. *Global Change Biol.*, 25, 1922-  
718 1940, <https://doi.org/10.1111/gcb.14619>.

719 Piao, S., Wang, X., Wang, K., Li, X., Bastos, A., Canadell, J. G., et al. (2019a). Interannual  
720 variation of terrestrial carbon cycle: Issues and perspectives. *Global Change Biol.*, 26, 300-  
721 318, <https://doi.org/10.1111/gcb.14884>.

722 Reichstein, M., Bahn, M., Ciais, P., Frank, D., Mahecha, M. D., Seneviratne, S. I., et al. (2013).  
723 Climate extremes and the carbon cycle. *Nature*, 500, 287-295,  
724 <https://doi.org/10.1038/nature12350>.

725 Reichstein, M., Falge, E., Baldocchi, D., Papale, D., Aubinet, M., Berbigier, P., et al. (2005). On  
726 the separation of net ecosystem exchange into assimilation and ecosystem respiration:  
727 review and improved algorithm. *Global Change Biol.*, 11, 1424-1439,  
728 <https://doi.org/10.1111/j.1365-2486.2005.001002.x>.

729 Rödenbeck C., Zaehle, S., Keeling, R., & Heimann, M. (2018). History of El Niño impacts on  
730 the global carbon cycle 1957-2017: a quantification from atmospheric CO<sub>2</sub> data. *Phil. Trans.  
731 R. Soc., B*, 373, 20170303, <https://doi.org/10.1098/rstb.2017.0303>.

732 Saigusa, N., Yamamoto, S., Hirata, R., Ohtani, Y., Ide, R., Asanuma, J., et al. (2008). Temporal  
733 and spatial variations in the seasonal patterns of CO<sub>2</sub> flux in boreal, temperate, and tropical  
734 forests in East Asia. *Agric. For. Meteorol.*, 148, 700-713. <https://doi.org/10.1016/j.agrformet.2007.12.006>.

736 Saigusa, N., Yamamoto, S., Murayama, S., & Kondo, H. (2005). Interannual variability of  
737 carbon budget components in an AsiaFlux forest site estimated by long-term flux  
738 measurements. *Agric. For. Meteorol.*, 134, 4-16.  
739 <https://doi.org/10.1016/j.agrformet.2005.08.016>.

740 Saigusa, N., Yamamoto, S., Murayama, S., Kondo, H., & Nishimura, N. (2002). Gross primary  
741 production and net ecosystem production of a cool-temperate deciduous forest estimated by  
742 the eddy covariance method. *Agric. For. Meteorol.*, 112, 203-215.  
743 [https://doi.org/10.1016/S0168-1923\(02\)00082-5](https://doi.org/10.1016/S0168-1923(02)00082-5).

744 Saitoh, T. M., Nagai, S., Noda, H. M., Muraoka, H., & Nasahara, K. N. (2012). Examination of  
745 the extinction coefficient in the Beer–Lambert law for an accurate estimation of the forest  
746 canopy leaf area index. *For. Sci. Tech.*, 8, 67-76,  
747 <https://doi.org/10.1080/21580103.2012.673744>.

748 Urbanski, S., Barford, C., Wofsy, S., Kucharik, C., Pyle, E., Budney, J., et al. (2007). Factors  
749 controlling CO<sub>2</sub> exchange on timescales from hourly to decadal at Harvard Forest. *J.*  
750 *Geophys. Res.*, 112, G02020, <https://doi.org/10.1029/2006JG000293>.

751 Wehr, R., Munger, J. W., McManus, J. B., Nelson, D. D., Zahniser, M. S., Davidson, E. A., et  
752 al. (2016). Seasonality of temperate forest photosynthesis and daytime respiration, *Nature*,  
753 534, 680-683, <https://doi.org/10.1038/nature17966>.

754 Wilson, K. B., Baldocchi, D. D., & Hanson, P. J. (2000), Spatial and seasonal variability of  
755 photosynthetic parameters and their relationship to leaf nitrogen in a deciduous forest. *Tree*  
756 *Physiol.*, 20, 565–578, <https://doi.org/10.1093/treephys/20.9.565>.

757 Wofsy, S. C., Goulden, M. L., Munger, J. W., Fan, S.-M., Bakwin, P. S., Daube, B. C., et al.  
758 (1993). Net Exchange of CO<sub>2</sub> in a Mid-Latitude Forest, *Science*, 260, 1314 – 1317,  
759 <https://doi.org/10.1126/science.260.5112.1314>.

760 Yamamoto, S., Murayama, S., Saigusa, N., & Kondo, H. (1999), Seasonal and inter-annual  
761 variation of CO<sub>2</sub> flux between a temperate forest and the atmosphere in Japan. *Tellus, Ser. B*,  
762 51, 402–413. <https://doi.org/10.1034/j.1600-0889.1999.00020.x>.

763 Yamamoto, Y., Ichii, K., Ryu, Y., Kang, M., Murayama, S., Kim, S.-J., & Cleverly, J. R. (2023).  
764 Detection of vegetation drying signals using diurnal variation of land surface temperature:  
765 Application to the 2018 East Asia heatwave. *Remote Sensing of Environment*, 291, 113572,  
766 <https://doi.org/10.1016/j.rse.2023.113572>.

767 Zani, D., Crowther, T. W., Mo, L., Renner, S. S., & Zohner, C. M. (2020). Increased growing-  
768 season productivity drives earlier autumn leaf senescence in temperate trees. *Science*, 370,  
769 1066–1071, <https://doi.org/10.1126/science.abd8911>.

770

771 Figure captions

772 **Figure 1.** a) Temporal variation in daily NEP (dot) and the best fit curve to the data (red line)  
773 for 1994-2021. b) Temporal variations in monthly mean daily NEP (red line), Rec (black  
774 line) and GPP (blue line) for the same period.

775 **Figure 2.** Temporal variations in annual NEP, Rec and GPP. The data were obtained by using  
776 an aerodynamic (AD) method and an eddy-covariance (EC) method until July 1998 and  
777 after that, respectively.

778 **Figure 3.** Schematic diagram showing factors governing the IAV in annual NEP; a) the IAV in  
779 the magnitude of the NEP during the summertime, and b) that in the length of the period  
780 (NGP) showing positive NEP values (between the NGS and the NGE).

781 **Figure 4.** Correlation coefficients (R) of the IAV between annual NEP and monthly mean NEP  
782 for each month for 1999-2021 (green and black vertical bars), and the averages of monthly  
783 mean NEP for each month over 1999-2021 (red closed circles) along with the standard  
784 deviation ( $1\sigma$ ) from the average values (red vertical lines). The green bars represent  
785 significant correlations at >99% confident levels.

786 **Figure 5.** IAVs in occurrences of NGS, NGE, LE<sub>LAI</sub>, LF<sub>LAI</sub>, LE<sub>CET</sub> and LF<sub>CET</sub>. LE<sub>LAI</sub> and LF<sub>LAI</sub>  
787 for 2019 are not plotted because of no available LAI data.

788 **Figure 6.** IAVs and significant trends of a) the monthly mean NEP, b) the monthly mean GPP  
789 of June-September, and c) the occurrences of the NGS (blue) and the NGE (red) and the  
790 length of the NGP (black).

791 **Figure 7.** IAVs and significant trends in a) the monthly mean LAI, b) the monthly mean solar  
792 radiation, c) the monthly mean daytime (11:00-17:00) VPD of June-September, and d) the  
793 spring (from March to May) mean and the August monthly mean air temperatures.

794 **Figure 8.** a) Comparison of IAVs in the monthly mean GPP of June-September between the  
795 observation and the simulation based on a multiple regression analysis, and b) IAVs in  
796 difference of the monthly mean GPP between the observation and the simulation.

797 **Figure 9.** IAVs in mean air temperature from March to May (black) and solar radiation in  
798 September (red). Pink-shades represent El Niño periods.

799

800 Table captions

801 **Table 1.** Correlation coefficient of IAVs of monthly mean SR in June, July, August and  
802 September with those of monthly mean NEP and GPP for the respective months in 1999-  
803 2021 and 1999-2017 except for 2004.

804 **Table 2.** Correlation coefficients (R) of IAV in monthly mean LAI for each of June, July, August  
805 and September with those in monthly mean NEP and GPP for the respective months and with  
806 those in annual NEP and GPP in the same year in 1999-2021 except for 2019 and in 1999-  
807 2017.

808 **Table 3.** Correlation coefficient (R) of IAVs in NGS, NGE and NGP with those of annual NEP

809 and GPP and environmental factors for 1999-2021 and 1999-2017.

810 **Table 4.** Correlation coefficients (R) of IAVs between interseasonal parameters for each period.